Technical Report

TR-99-27

The effect of hydrogen and gamma radiation on the oxidation of UO_2 in 0.1 mol · dm^{-3} NaCl solution

King F, Quinn M J, Miller N H

AECL, Whiteshell Laboratories
Pinawa, Manitoba

November 1999

Svensk Kärnbränslehantering AB
Swedish Nuclear Fuel
and Waste Management Co
Box 5864
SE-102 40 Stockholm Sweden
Tel 08-459 84 00
+46 8 459 84 00
Fax 08-661 57 19
+46 8 661 57 19

The effect of hydrogen and gamma radiation on the oxidation of UO_2 in 0.1 mol · dm^{-3} NaCl solution

King F, Quinn M J, Miller N H

AECL, Whiteshell Laboratories
Pinawa, Manitoba

November 1999

This report concerns a study which was conducted for SKB. The conclusions and viewpoints presented in the report are those of the author(s) and do not necessarily coincide with those of the client.

Abstract

High partial pressures of H_2 may develop in an underground nuclear fuel waste disposal vault as a result of radiolysis of groundwater or corrosion of steel container components. The presence of H_2 could suppress the oxidation and subsequent dissolution of used fuel by creating reducing conditions near the fuel surface.

A series of experiments has been performed to determine the extent of oxidation of UO_2 due to γ-radiolysis in the presence of H_2. A H_2 partial pressure of 5 MPa was used to simulate the maximum possible pressure of H_2 in a disposal vault located at a depth of 500 m. Experiments were also performed with an Ar overpressure for comparison. Deaerated 0.1 $mol \cdot dm^{-3}$ NaCl was used to simulate the groundwater. The extent of oxidation was determined by monitoring the corrosion potential of UO_2 electrodes, by cathodically stripping the oxidized layer from the electrode at the end of the test, and by determining the ratio of U(VI) to U(IV) species on the surface of a UO_2 disc exposed to the same solution by X-ray photoelectron spectroscopy.

The presence of H_2 is found to have two effects on the oxidation of UO_2 in the presence of γ-radiation. Not only does H_2 prevent oxidation of the UO_2 by radiolytic oxidants but it also produces more reducing conditions than those observed with either H_2 or Ar atmospheres in the absence of irradiation. It is suggested that radiolytically produced reductants participate in homogeneous reactions in solution with radiolytic oxidants and in heterogeneous reactions on the UO_2 surface, most likely at reactive grain-boundary sites.

Contents

List of tables

List of figures

1 Introduction

There is increasing evidence that the presence of dissolved hydrogen suppresses the oxidative dissolution of UO_2 and used nuclear fuel. Experiments with used fuel show that high H_2 overpressures (5 MPa) suppress the rate of fuel dissolution /K Spahiu, private communication, 1998/. Modelling calculations by Eriksen /1996/ suggest that the rate of fuel dissolution (as indicated by the rate of oxidant consumption) should decrease as the concentration of hydrogen increases, as a consequence of the effect of hydrogen on radical recombination reactions.

Hydrogen could be present in a nuclear fuel waste container as a result of either radiolysis of the groundwater or corrosion of the container. Molecular hydrogen forms radiolytically by the recombination of H• radicals and, being relatively stable, tends to accumulate in the system during radiolysis experiments. Corrosion of C-steel container components under anaerobic conditions also produces molecular H_2. The concentration of dissolved H_2 at the fuel surface will depend upon the relative rates of formation of H_2 and its mass transport away from the container, as well as the partial pressure of H_2 at vault depth. Given that the rate of diffusive mass transport of H_2 away from the container is limited, the concentration of dissolved H_2 is expected to quickly exceed the solubility of H_2 in groundwater. The dissolved [H_2] will then depend on the partial pressure of gaseous H_2, which will have a maximum value equal to the hydrostatic pressure at vault depth (5 MPa at 500 m).

Electrochemical measurements of the corrosion potential (E_{CORR}) of UO_2 combined with surface analysis using X-ray photoelectron spectroscopy (XPS) provide a sensitive method for determining the extent of oxidation of UO_2 surfaces /Shoesmith et al, 1994/. The degree of surface oxidation is a function of potential (E), with reversible oxidation of the surface (as UO_{2+x}) occurring for $E < -0.4\ V_{SCE}$, irreversible oxidation of the surface [up to $UO_{2.33}$ (U_3O_7)] occurring at more positive potentials, and oxidative dissolution as U(VI) occurring at $E \geq -0.1\ V_{SCE}$. XPS can be used to provide a quantitative analysis of the degree of oxidation in the first few layers on the surface. Deconvolution of the U peak in the XPS signal is used to determine the U(VI):U(IV) ratio in the surface layers.

This report describes the results of a series of electrochemical and XPS experiments on the effects of H_2 on the oxidation of UO_2 in the presence of γ-radiation. The experiments were conducted in deaerated 0.1 mol·dm^{-3} NaCl at room temperature, using atmospheres of either Ar or H_2 at a pressure of 5 MPa. The solution was irradiated using a sealed ^{192}Ir source. In addition to measuring the time dependence of E_{CORR}, the amount of precipitated U(VI) was determined at the end of each experiment by electrochemically reducing the surface oxide film. The degree of surface oxidation was determined by XPS on a separate UO_2 sample exposed to the same environment.

2 Experimental

The UO_2 electrode and coupons for the XPS analyses were cut from a single UO_2 fuel pellet prepared at Whiteshell Laboratories for another experimental program. (A second electrode, prepared from a different pellet, was used in one of the electrochemical experiments). The density of the 20-mm-long by 14-mm-diameter pellet was ~95% of the theoretical density (10.95 $g \cdot cm^{-3}$). One 6-mm-long sample was cut from the centre of the pellet to prepare the electrode and two 3-mm-long samples were cut as discs for the XPS samples.

Figure 2-1 shows the design of the UO_2 electrode. The UO_2 disc was Cu-plated on one side and attached using conducting epoxy to a stainless steel stub, into which a Ti rod was inserted to provide an electrical contact. The Ti rod and the top of the stainless steel stub were insulated from the solution by a PTFE washer and two layers of heat-shrink plastic. The edge of the stub and UO_2 disc were wrapped with PTFE tape prior to each experiment to insulate the rest of the electrode assembly from the solution. The surface area of the exposed UO_2 disc was 1.54 cm^2. The electrical conductivity of the UO_2 disc (estimated from the Cu plating procedure) was 560 Ω. This resistance value is towards the lower end of the range found in previous studies for the resistance of natural UO_2 electrodes /200–2000 Ω, Hocking et al, 1991/, resulting in reliable electrochemical measurements. Prior to assembling each experiment, the exposed face of the UO_2 disc was lightly polished with 600-grit SiC paper and rinsed with water to remove polishing fines.

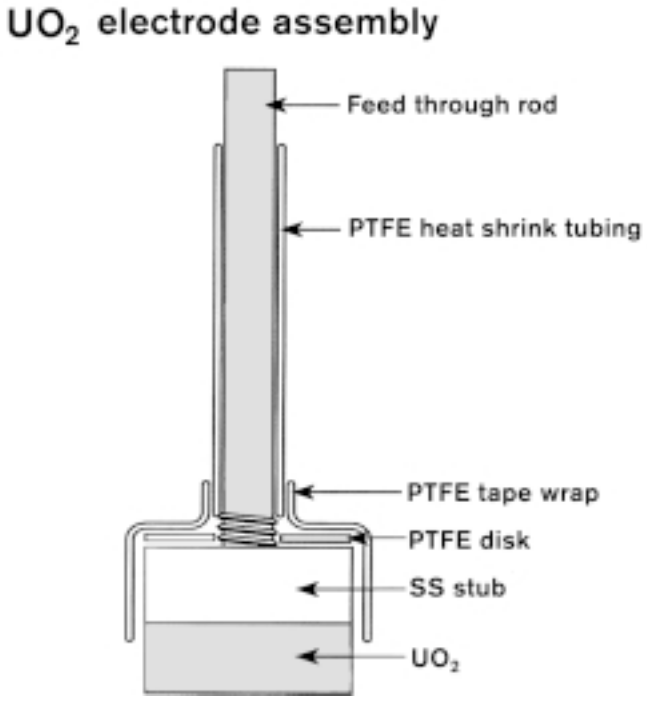

Figure 2-1. *Design of UO_2 electrode.*

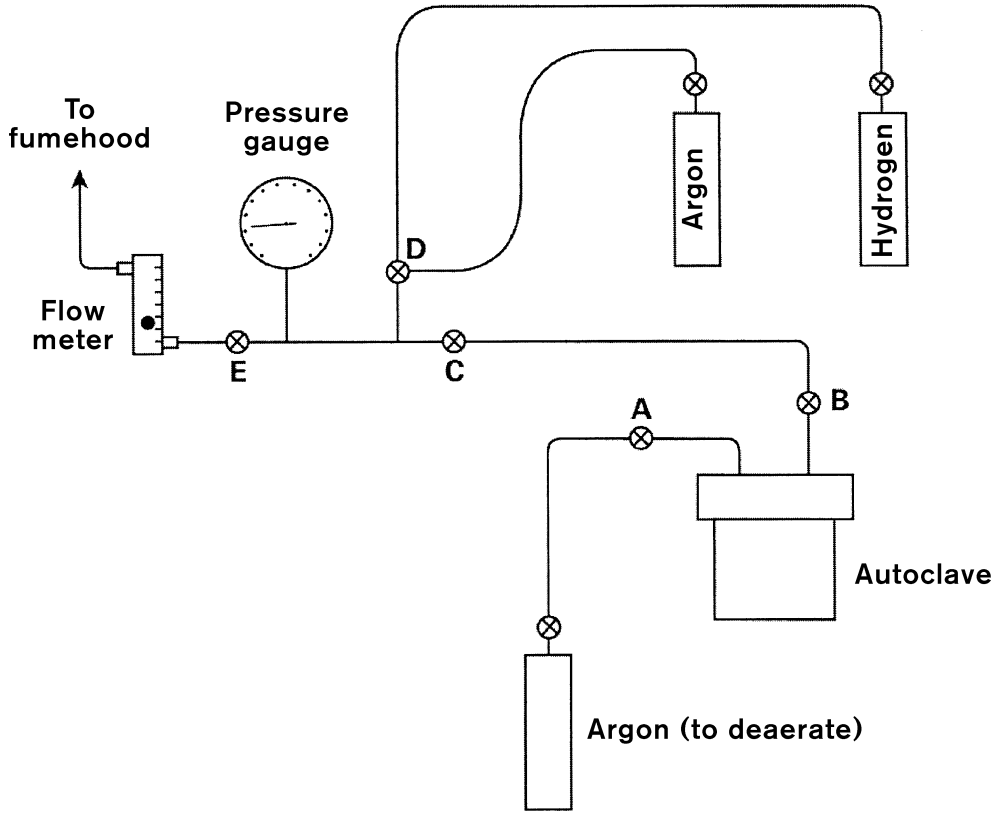

Figure 2-2. *Gas train used for purging and over-pressurizing pressure vessel.*

The UO_2 electrode was immersed in solution inside a 1-L Hastelloy-C pressure vessel (Parr Instruments, IL) which was placed in the irradiation chamber of a lead-lined "gamma castle." All experiments were conducted at ambient temperature (22±1°C). The castle was equipped with a sealed ^{192}Ir γ-source ($t_{1/2}$ = 74 d, initial activity 107 Ci (15 d prior to the first irradiated experiment), supplied by MDS Nordion, Kanata, Ontario) which could be remotely introduced into, and removed from, the irradiation chamber. When introduced into the chamber, the source was located directly beneath the pressure vessel, and directed towards the exposed face of the UO_2 electrode. Dosimetry performed inside the pressure vessel 6 d after the experimental campaign was completed gave an absorbed dose rate of 10.7 $Gy \cdot h^{-1}$. All irradiated experiments were completed within a 37-d period. Thus, the absorbed dose rates in the various experiments ranged from 15.9 $Gy \cdot h^{-1}$ (experiment SKB5) to 11.3 $Gy \cdot h^{-1}$ (experiment SKB13).

The pressure vessel was connected to a gas train to permit purging and over-pressurization with Ar or H_2 gas (Figure 2-2). Before and after each experiment, the pressure vessel was purged with high-purity Ar gas at atmospheric pressure (0.1 MPa) to degas the solution prior to electrochemical pre-treatment and cathodic-stripping voltammetry experiments (see below). During the experiments, the pressure vessel was filled with either Ar or H_2 gas at a pressure of 5.2 MPa (750 psi). In some irradiated experiments, the gas in the pressure vessel was switched from Ar to H_2, or vice versa, and the irradiation continued. The detailed procedure for the various degassing and over-pressurization operations is given in Appendix A. The gas line was designed and operated to avoid the possibility of contamination by atmospheric O_2 or residual H_2 (when switching from H_2 to Ar atmospheres during irradiation).

The electrode was immersed in a Pyrex glass liner containing deaerated 0.1 mol·dm^{-3} NaCl (volume 310 cm^3) prepared from AR-grade chemicals and distilled-deionized H_2O from a Millipore apparatus. The pH of the test solution was adjusted to pH 9.5 using dilute NaOH solution. A large-surface-area Pt mesh counter electrode and custom-designed 0.1 mol·dm^{-3} KCl/AgCl reference electrode were used. The potential of the reference electrode, designed to withstand the elevated pressure inside the vessel, was measured before and after each experiment and was found to have a potential of between –0.034 V_{SCE} and –0.042 V_{SCE}. Except where specifically noted, all potentials quoted in this report have been converted to the SCE scale. Problems were encountered with the reference electrode in some of the experiments, especially those involving switches in the over-pressurizing gas, resulting in loss of potential signal.

A list of the experiments performed is given in Table 2-1. The experiments were performed sequentially, with a period of 2–3 d between the start of successive irradiated experiments (SKB5-13).

Table 2-1. Summary of experiments performed on the effect of H_2 on the oxidation of UO_2 in the presence of γ-irradiation.

Experiment #	Over-pressurizing gas Stage 1	Over-pressurizing gas Stage 2	Irradiation
SKB1	Ar	-	N
SKB2	Ar	-	N
SKB3	H_2	-	N
SKB4	H_2	-	N
SKB5	H_2	-	Y
SKB6	H_2	-	Y
SKB7	H_2	-	Y
SKB8	H_2	Ar	Y
SKB9	Ar	H_2	Y
SKB10	H_2	Ar	Y
SKB11	Ar	-	Y
SKB12	Ar	H_2	Y
SKB13	Ar	-	Y

The following general procedure was used for each of the thirteen experiments. The assembled pressure vessel, containing the UO_2 electrode and a 3-mm-thick slice of UO_2 for surface analysis, was placed inside the irradiation chamber and attached to the gas train. The solution inside the pressure vessel was deaerated by bubbling Ar at atmospheric pressure for 30 min. With the gas still flowing to remove traces of O_2 or H_2 gas produced during electrolysis, the UO_2 electrode was cathodically cleaned at –2.0 $V_{Ag/AgCl}$ for 5 min to remove surface films present on the surface after polishing or formed on the surface from reaction with residual dissolved O_2 prior to deaeration.

Following cathodic cleaning, the pressure vessel was over-pressurized with the appropriate gas, the ^{192}Ir source extended into the irradiation chamber (for irradiated experiments) and E_{CORR} monitored at 5-min intervals. Measurements were made until a steady-state E_{CORR} was achieved (generally 18–24 h). At this stage, if the experiment was to be continued with the other gas, the pressure vessel was refilled with the other over-

pressurizing gas and E_{CORR} monitored again during the second stage of the experiment until a steady-state potential had once again become established (generally a further 18–24 h). In some experiments in which the over-pressurizing gas was switched for the other gas, the ^{192}Ir source was retracted for ~10 min to enable the valves located inside the irradiation chamber to be opened and closed. In two experiments, gas samples were taken at the end of the experiment for analysis by mass spectrometry.

At the end of the experiment, the pressure inside the vessel was relieved and Ar bubbled through at atmospheric pressure for 30 min. Before disassembly of the vessel, the surface films formed on the UO_2 electrode were removed using cathodic-stripping voltammetry (CSV). The potential of the electrode was scanned from a potential close to the final E_{CORR} in a cathodic (reducing) direction at a rate of 10 $mV \cdot s^{-1}$ to a potential of –2.0 $V_{Ag/AgCl}$ and back again to the original potential. The quantity of precipitated surface oxides was then estimated by integration of the current-time (or E) curve.

Following the CSV, the pressure vessel was sealed, removed from the irradiation chamber and transferred to an anaerobic chamber. There, the pressure vessel was opened, the thin UO_2 disc removed from the bottom of the liner, the surface rinsed with distilled-deionized H_2O and the disc placed inside a transfer cell. The sealed transfer cell was attached to the X-ray photoelectron spectrometer for analysis of the extent of oxidation of the uppermost surface of the UO_2 disc exposed to the solution in the pressure vessel. In this way, the UO_2 disc was not exposed to atmospheric O_2 prior to XPS analysis. The XPS spectra were recorded using an ESCA-5300 system (Perkin-Elmer), with both high-resolution U 4f, C 1s and O 1s and valence-band regions recorded. Deconvolution of the U-$4f_{7/2}$ peak was used to estimate the ratio of U(VI) to U(IV) species on the surface of the disc /Sunder et al, 1990/.

3 Results

3.1 E_{CORR} measurements

The E_{CORR} was measured during the course of each of the experiments listed in Table 2-1. Table 3-1 lists the steady-state E_{CORR} value(s), and other parameters, measured for each experiment. The individual E_{CORR} vs. time plots are given in Appendix B. All plots show the same general behaviour of a rapid increase in E_{CORR} over the first 100–200 min followed, in most cases, by a slower attainment of an apparent steady-state potential. Steady-state was not established, however, within ~20 h for the case of irradiated experiments with a H_2 overpressure (see below).

Figures 3-1 and 3-2 compare the effects of Ar and H_2 overpressures in unirradiated and irradiated solutions, respectively. In the absence of γ-radiation (Figure 3-1), there was relatively little difference between the E_{CORR} values for the two gases, especially for experiments SKB2 (Ar) and SKB4 (H_2), for which the final steady-state E_{CORR} values differed by only 0.02 V. Thus, at room temperature, Ar and H_2 appear to have a similar effect on the extent of oxidation of UO_2. By comparison with previous studies /Shoesmith et al, 1994/, the steady-state E_{CORR} of ~-0.4 V_{SCE} corresponds approximately to the limit below which the surface undergoes reversible oxidation.

In irradiated solution, E_{CORR} was significantly more positive in solutions over-pressurized with Ar than with H_2 (Figure 3-2). (Figure 3-2 shows the results of all irradiated single-stage experiments, as well as the first stage of those experiments in which the over-pressurizing gas was changed). In the presence of Ar (SKB9, 11, 12 and 13), steady-state

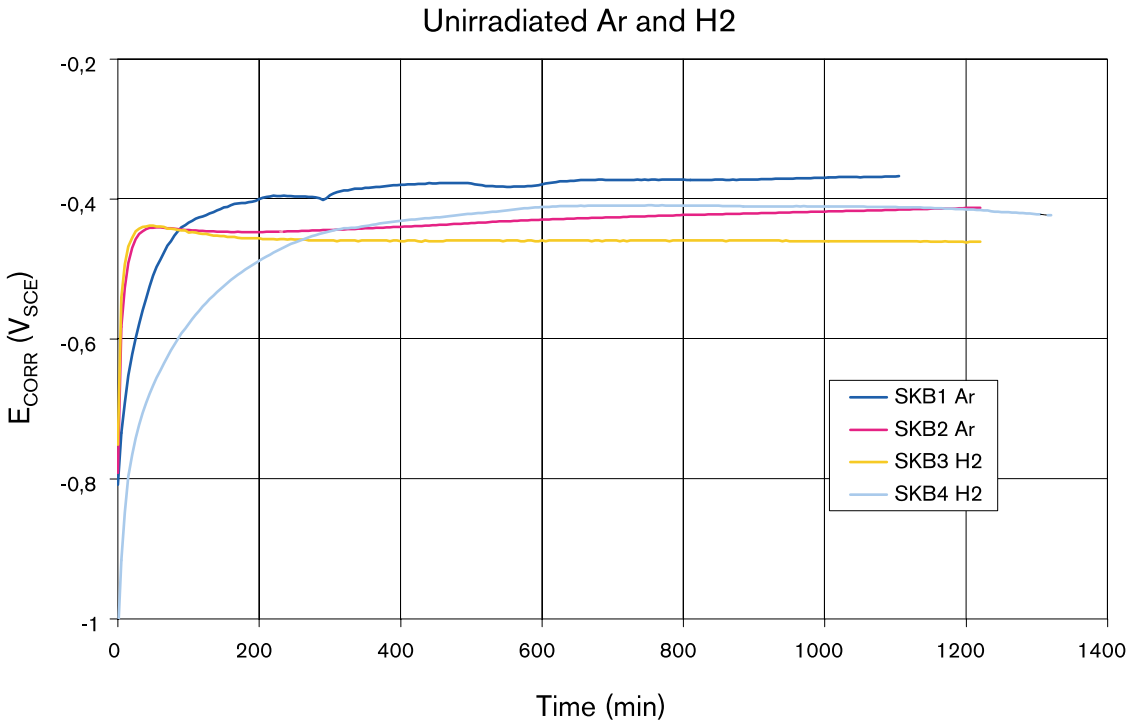

Figure 3-1. *Time dependence of the corrosion potential of UO_2 in unirradiated solution with Ar and H_2 overpressures.*

Table 3-1. The effect of γ-radiolysis and gas atmosphere on the oxidation of UO_2.

Expt #	γ-dose rate	Stage 1		Stage 2		E_{CORR} (V_{SCE})[1]		U(VI):U(IV)	Q (mC)	pH	
	($Gy \cdot h^{-1}$)	Gas	Time(h)	Gas	Time(h)	Stage 1	Stage 2			Before	After
SKB1		Ar	19.3	-	-	-0.37	-	0.35	[2]	9.5	6.4
SKB2		Ar	20.3	-	-	-0.41	-	0.30	0	9.5	9.0
SKB3		H_2	20.3	-	-	-0.4 6	-	0.25	0	9.5	9.3
SKB4		H_2	22.0	-	-	-0.43	-	0.40	[2]	9.5	8.8
SKB5	15.9	H_2	19.9	-	-	-0.55	-	0.42	[2]	9.5	9.1
SKB6	15.4	H_2	21.4	-	-	-0.8 0	-	0.42	0	9.5	-
SKB7	14.9	H_2	21.5	-	-	-0.6 6	-	0.32	[2]	9.5	9.2
SKB8	14.4	H_2	22.0	Ar	23.5	-0.86	-0.50	0.33	[3]	9.5	8.8
SKB9	13.7	Ar	23.0	H_2	21.0	-0.34	-0.59	0.53	[3]	9.5	8.3
SKB10	12.8	H_2	22.5	Ar	23.5	-0.50	-0.42	0.34	[3]	9.5	8.7
SKB11	12.3	Ar	19.0	-	-	-0.26	-	0.43	[3]	9.5	8.7
SKB12	12.0	Ar	23.0	H_2	22.5	-0.27	-0.51	0.30	0.93	9.5	8.5
SKB13	11.3	Ar	20.2	-	-	-0.29	-	0.71	[3]	9.5	9.0

[1]At steady state or at the end of the test if steady state not achieved.

[2]No well-defined reduction peak.

[3]Failed reference electrode or noisy signal.

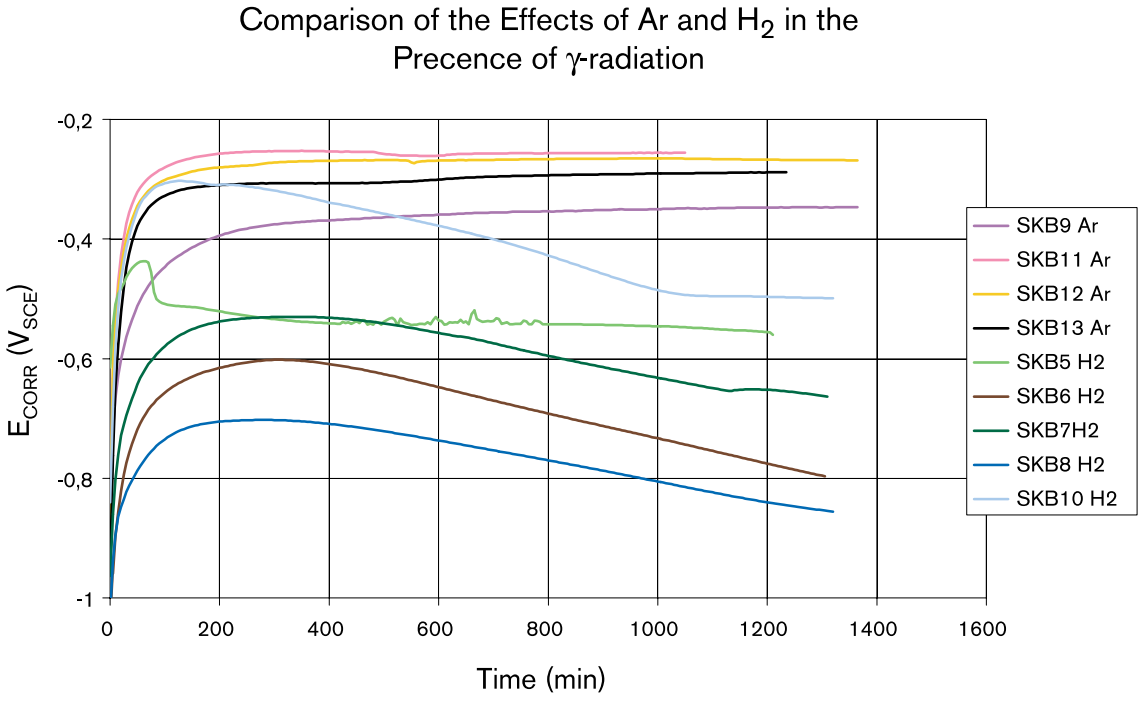

Figure 3-2. *Time dependence of the corrosion potential of UO_2 in irradiated solution with Ar and H_2 overpressures.*

E_{CORR} values more positive than -0.34 V_{SCE} were observed. At these potentials, the surface would be expected to be undergoing irreversible oxidation, although the measured E_{CORR} values are still more negative than the potential threshold for the oxidative dissolution of UO_2 (-0.1 V_{SCE}). In the presence of H_2 (SKB5, 6, 7, 8, 10), E_{CORR} values more negative than -0.50 V_{SCE} were observed, with the most negative E_{CORR} value being –0.86 V_{SCE} (SKB 8). In at least two of the irradiated H_2 experiments (SKB6 and 8), the E_{CORR} had not reached steady state after 22 h irradiation. Thus, in the presence of H_2, the E_{CORR} values were a minimum of 0.16 V, and as much as 0.6 V, more negative than those observed in irradiated solutions over-pressurized with Ar.

The effect of irradiation for the two gases is shown in Figures 3-3 and 3-4, which compare irradiated and unirradiated experiments for the Ar and H_2 overpressures, respectively. For Ar (Figure 3-3), irradiation causes a positive shift in E_{CORR} to more-oxidizing values. The difference in steady-state E_{CORR} values is as much as 0.15 V. In contrast, in H_2 over-pressurized systems, irradiation cause a negative shift in E_{CORR} to more-reducing values (Figure 3-4). The difference in "steady-state" E_{CORR} values is as much as 0.43 V, although there is a tendency in irradiated H_2 environments for the E_{CORR} to attain steady-state more slowly than in either unirradiated or irradiated Ar-containing environments.

The difference in behaviour in irradiated solution between Ar- and H_2-containing environments is shown more clearly by the results of the two-stage experiments in which the over-pressurizing gas was changed during the course of the experiment (Figure 3-5). After the initial rise, E_{CORR} becomes more negative in H_2-containing systems (SKB 8 and 10), but reaches a relatively positive steady-state value in Ar-containing solution (SKB9 and 12). Upon changing the over-pressurizing gas, E_{CORR} shifts in the oxidizing direction when H_2 is changed to Ar and in the reducing direction when Ar is changed to H_2. In both cases, however, the change in E_{CORR} occurs simultaneously (within 5 min) with the change in gas atmosphere.

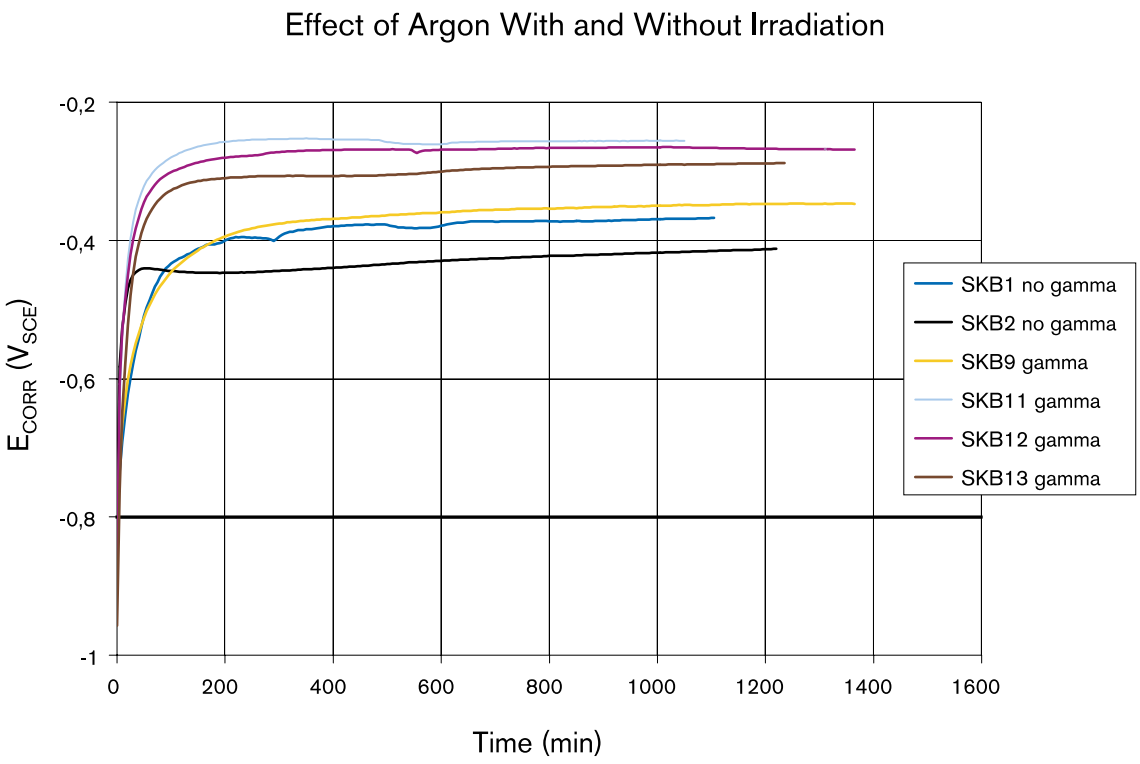

Figure 3-3. *Effect of γ-irradiation on the time dependence of the corrosion potential of UO_2 in solution with an Ar overpressure.*

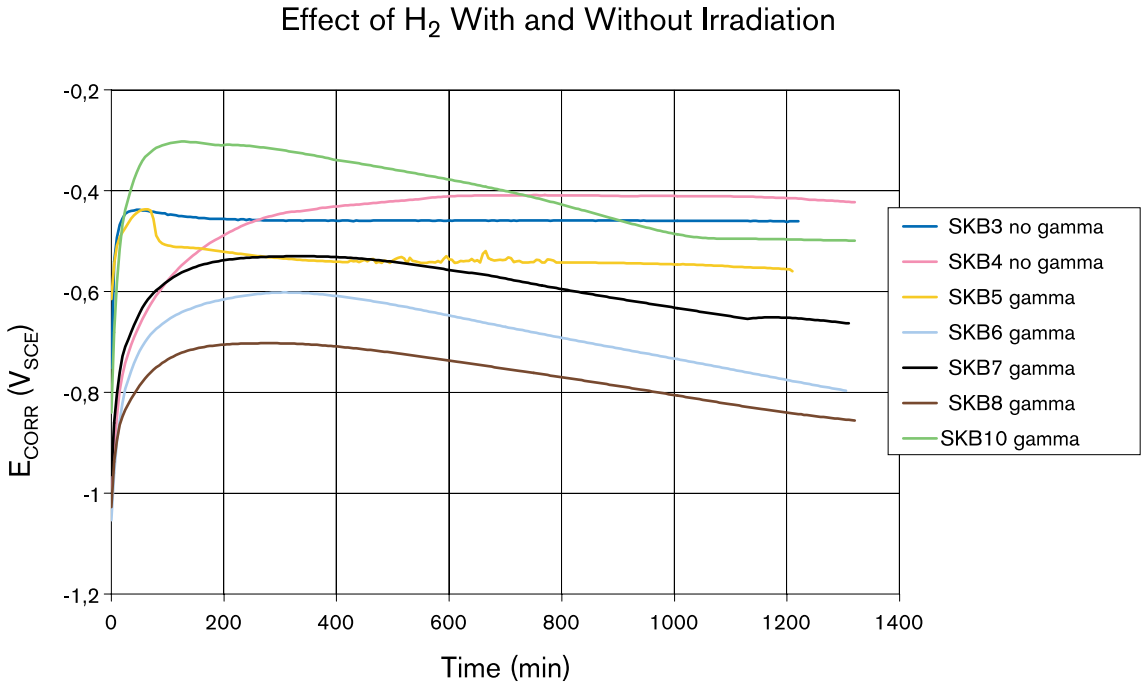

Figure 3-4. *Effect of γ-irradiation on the time dependence of the corrosion potential of UO_2 in solution with a H_2 overpressure.*

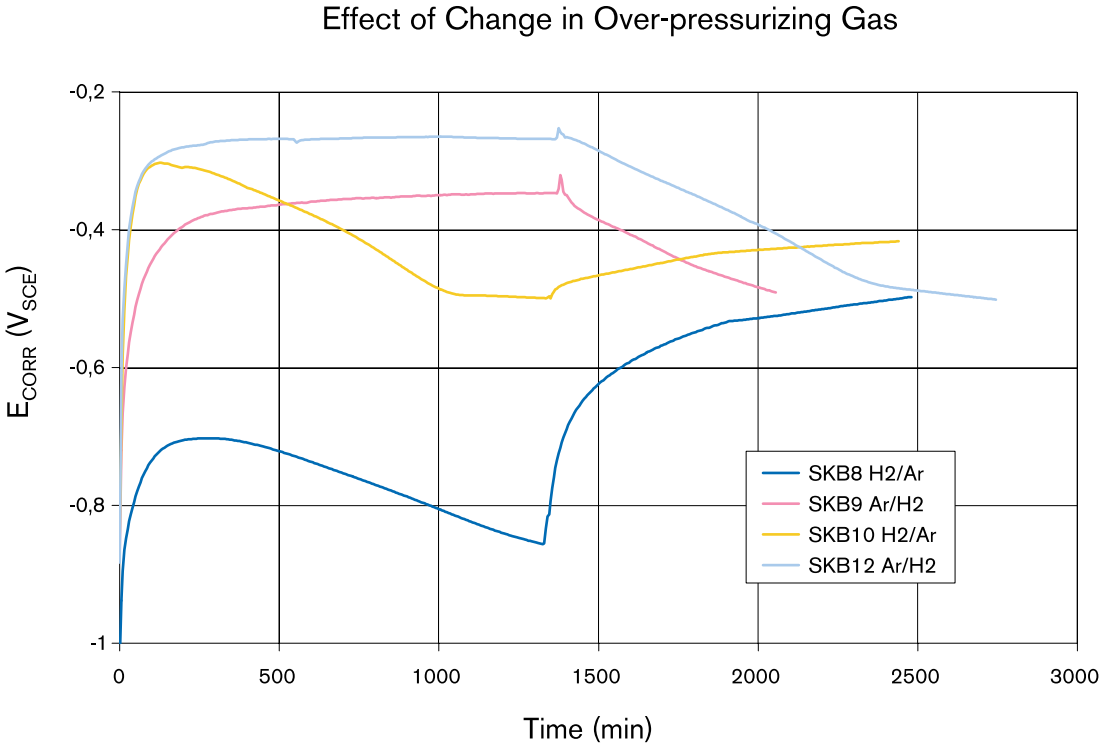

Figure 3-5. *Effect of changing gas overpressure on the corrosion potential of UO_2 in irradiated solution. In experiments SKB8 and 10, the initial H_2 overpressure was changed to Ar after ~1300 min. In experiments SKB9 and 12, the initial Ar overpressure was changed to H_2 after ~1400 min.*

The measured E_{CORR} values are, in general, significantly more negative than those previously observed on UO_2 (see below). To investigate whether this was the result of having manufactured the UO_2 electrode from a particularly unreactive UO_2 pellet, a second electrode from a different pellet was used for experiment SKB6 (irradiated, H_2 atmosphere). Figure 3-6 shows that the second electrode used (E2, experiment SKB6) gave results intermediate between those of experiments with the electrode from this study (S1, experiments SKB5, 7, 8 and 10).

Although the experiments were performed sequentially, and therefore at different dose rates, there is no evidence for any dose-rate dependence over the limited range of dose rates used here (15.9–11.3 $Gy \cdot h^{-1}$). For example, the most negative steady-state E_{CORR} value recorded in irradiated Ar-over-pressurized solution was that measured with the highest activity source (SKB 9, compared with SKB11, 12 and 13). Similarly, since irradiation causes a negative shift in E_{CORR} in H_2-containing solution, E_{CORR} would be expected to be more negative in experiment SKB5 than in subsequent experiments, which was found not to be the case (Table 3-1).

The initial rate of oxidation was determined from the slopes of E_{CORR} as a function of log t (Figure 3-7). These curves were found to be linear over the initial 35–100 min for each experiment. This period corresponds to the initial oxidation of the cathodically cleaned UO_2 electrode. Table 3-2 summarizes the slopes for the various experiments, determined over the initial 35-100 min for each curve. In unirradiated solution, there is little difference between Ar- and H_2-containing systems in the rate of initial oxidation [mean slopes of 0.21 V and 0.19 V, respectively (experiments SKB1-4)]. In irradiated solution, however, the UO_2 electrodes in Ar-containing solution oxidized slightly faster

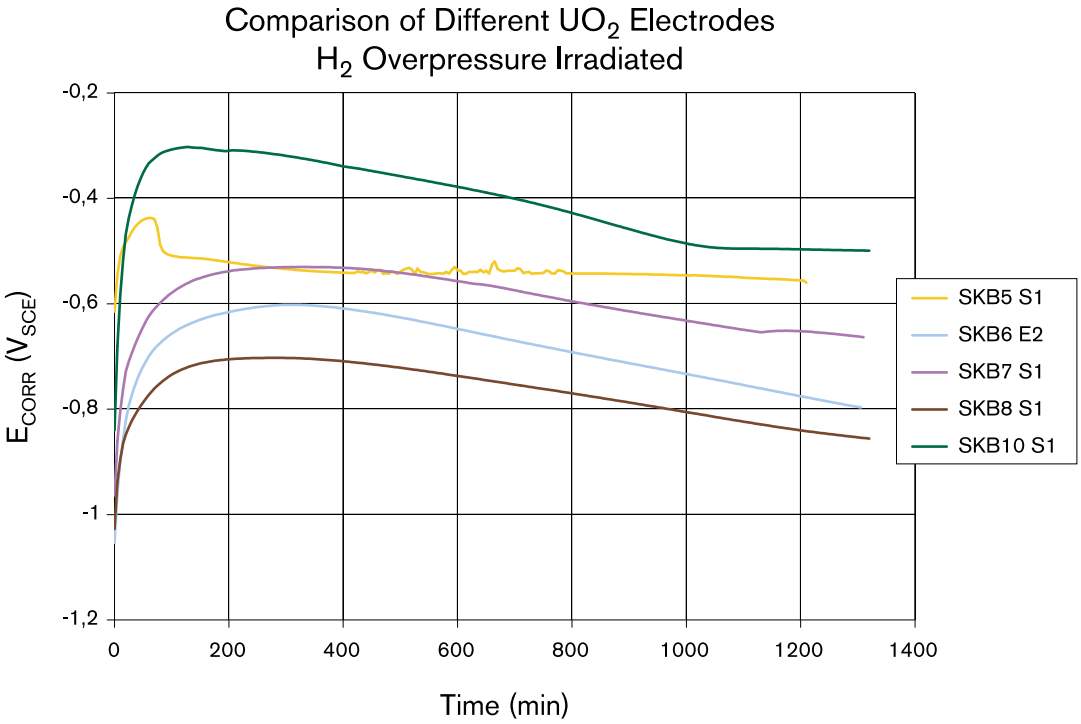

Figure 3-6. *Comparison of the effect of H_2 on the corrosion potential of UO_2 in irradiated solution with different electrodes.*

Table 3-2. Initial rate of oxidation of UO_2 electrodes.

Experiment #	Over-pressurizing gas	Irradiation	Slope[1]
SKB1	Ar	N	0.253
SKB2	Ar	N	0.167
SKB3	H_2	N	0.121
SKB4	H_2	N	0.260
SKB5	H_2	Y	0.103
SKB6	H_2	Y	0.241
SKB7	H_2	Y	0.221
SKB8	H_2	Y	0.158
SKB9	Ar	Y	0.217
SKB10	H_2	Y	0.344
SKB11	Ar	Y	0.333
SKB12	Ar	Y	0.269
SKB13	Ar	Y	0.406

[1]The slope is the value of $dE_{CORR}/d\log t$ over the initial 35-min or 100-min region in figure 3-7.

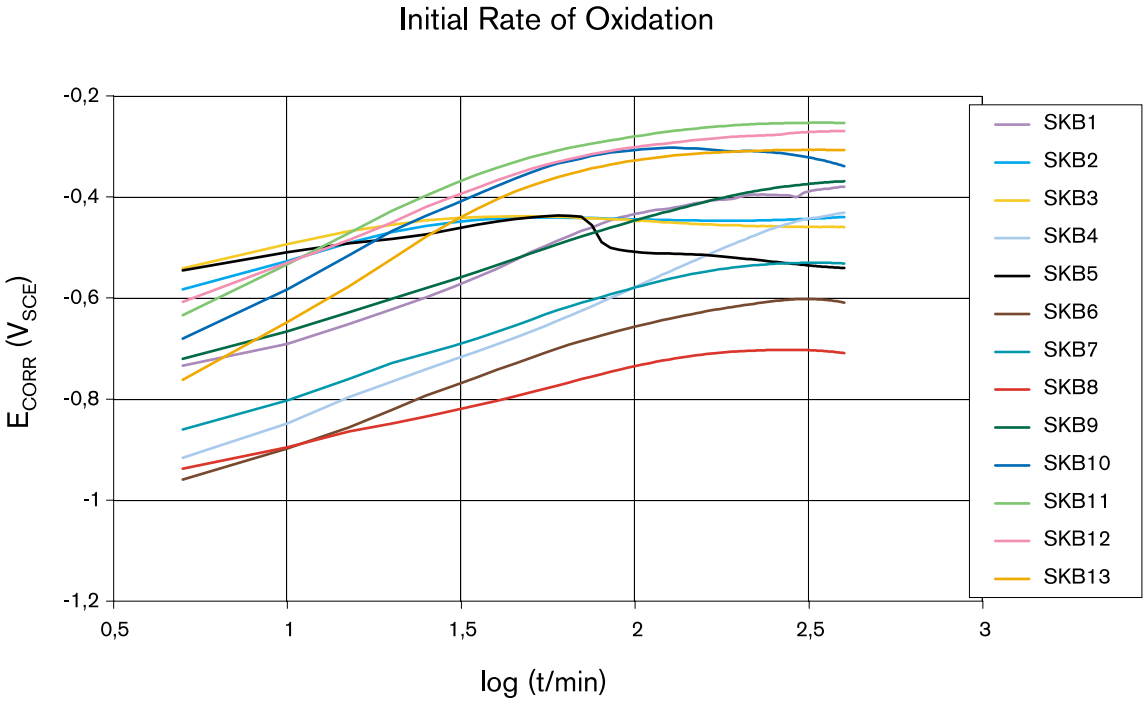

Figure 3-7. *Initial rate of oxidation of UO_2 electrodes.*

(mean slope 0.31 V) than the electrodes immersed in H_2-containing solution (mean slope 0.21 V). There was no dependence of the initial rate of oxidation on the magnitude of the initial potential, i.e., those electrodes with the most reduced surface (most negative initial E_{CORR} value) did not oxidize faster than those with more-positive initial E_{CORR} values (more-oxidized surface).

3.2 Cathodic stripping voltammetry

The results of the cathodic stripping voltammetry performed on the oxidized UO_2 electrodes at the end of the experiments are given in Table 3-1 as the equivalent reduction charge (Q). This charge is the integrated area under the peak observed in the voltammogram, and is a measure of the quantity of U(VI) precipitated on the electrode surface /Shoesmith and Sunder, 1991/. The technique was of limited usefulness in this study, however, for two reasons. First, in a number of the experiments (SKB8, 9, 10, 11 and 13), the reference electrode either failed during the course of the experiment or produced noisy voltammograms. Second, the limited extent of oxidation in many of the remaining experiments resulted in poorly defined reduction peaks, making it difficult to estimate a reduction charge. In fact, it was only possible to identify a definitive reduction peak in four experiments (SKB2, 3, 6 and 12), and in only one of those (SKB12) was there any measurable surface oxide.

3.3 XPS analyses

The degree of surface oxidation was also determined by XPS analysis of the uppermost surface of a UO_2 disc (i.e., the surface exposed to solution) placed in the bottom of the

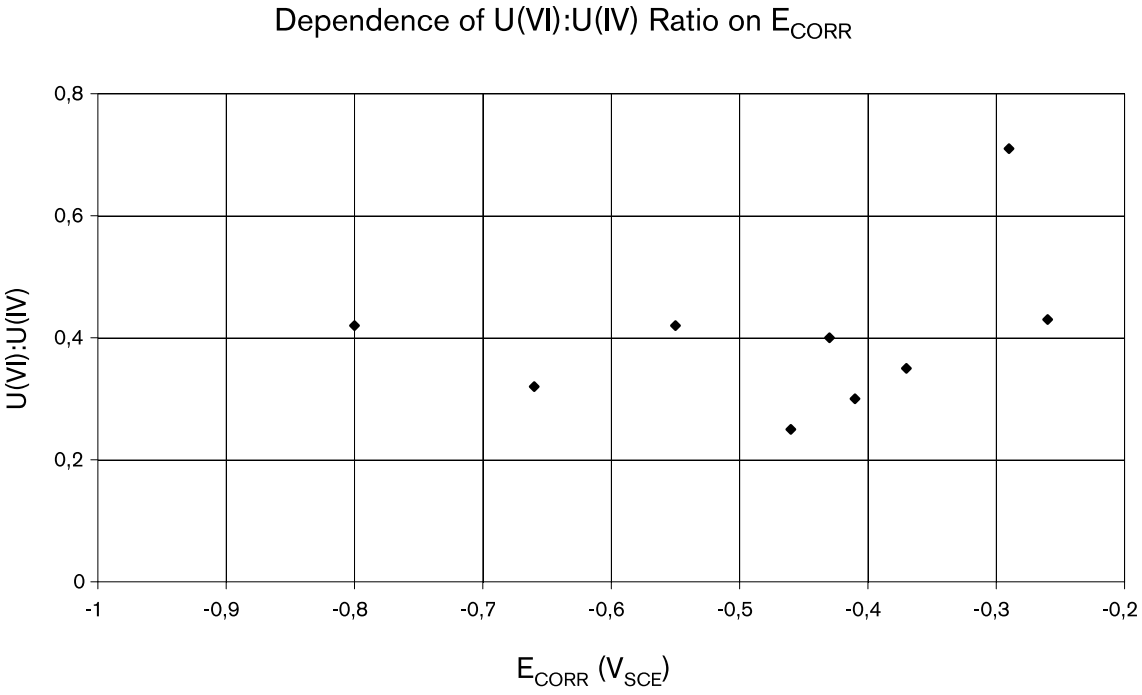

Figure 3-8. *Dependence of the observed U(VI):U(IV) ratio on the corrosion potential.*

experimental vessel. Two discs, cut from the same UO_2 pellet as the electrode, were used alternately, with one disc being used in an experiment while the other disc was being analyzed by XPS.

The U(VI):U(IV) ratio determined by XPS for each of the experiments is given in Table 3-1. In general, the XPS analyses showed little oxidation of the surface, consistent with both the relatively negative E_{CORR} values and the lack of evidence for precipitated U(VI) layers from the cathodic stripping voltammetry. There is no evidence from the XPS results that either of the two discs was more readily oxidized than the other. Because of the uncertainties associated with the deconvolution of the U-$4f_{7/2}$ peak, the sensitivity limit for this technique is a U(VI):U(IV) ratio of ~0.33, consistent with a surface layer of U_4O_9. From the mean estimated U(VI):U(IV) ratios for the various experimental conditions, it is apparent that there is no difference in the extent of surface oxidation in unirradiated solution for Ar and H_2 atmospheres. In irradiated solution, however, the mean U(VI):U(IV) ratio in Ar-containing solution (0.57) is higher than that in H_2-containing solution (0.39), consistent with the more positive E_{CORR} values observed in the former solution. Overall, however, there is little dependence of the estimated U(VI):U(IV) ratio on the steady-state E_{CORR} for experiments (irradiated and unirradiated) in which only a single over-pressurizing gas was used (Figure 3-8).

3.4 Solution pH and gas analyses

The solution pH, adjusted to pH 9.5 prior to the experiment by adding dilute NaOH solution, was invariably found to decrease during the experiment. In the extreme case (SKB1) the pH dropped to pH 6.4, but more usually the decrease was limited to ~1 pH unit (Table 3-1).

Table 3-3 shows the results of the two post-test gas analyses performed. The samples from experiments SKB11 and 13 show evidence for air contamination, although the O_2 content of SKB13 is higher than that which would be predicted based on the N_2 content. Both experiments were irradiated for ~20 h with Ar atmospheres, with one (SKB13) showing considerably more H_2 formation than the other (SKB11).

Table 3-3. Post-test gas analyses.

	H_2 (vol. %)	N_2 (vol. %)	O_2 (vol. %)	Ar (vol. %)
SKB11	<0.001	0.36	0.08	99.6
SKB13	0.21	4.72	2.23	92.8

4 Discussion

The extent of surface oxidation of a UO_2 electrode varies with the potential of the surface /Shoesmith et al, 1994/. Three regions can be identified:

$E < -0.4\ V_{SCE}$ the surface undergoes reversible oxidation,

$E > -0.4\ V_{SCE}$ the surface undergoes irreversible oxidation,

$E = -0.1\ V_{SCE}$ surface composition corresponds to $UO_{2.33}$ (U_3O_7), taken to be the threshold for oxidative dissolution.

The term "reversible oxidation" refers to the observation from electrochemical experiments that the response of the electrode is the same if the potential is scanned in the positive (oxidation) or negative (reduction) direction. These observations have been made in both conventional voltammetric experiments, in which the amount of material oxidized (as measured by the area under the current-potential plot for the oxidation scan) is equal to the amount of material reduced on the subsequent reduction scan, and in photoelectrochemical tests, in which the photocurrent is identical in the oxidation and reduction scans provided the potential is not scanned more positive than $-0.4\ V_{SCE}$. It is believed that in this potential region ($E < -0.4\ V_{SCE}$), oxidation occurs at specific surface sites, most probably located at grain boundaries /D W Shoesmith, private communication, 1999/. Much of the non-stoichiometry of the electrode is located at the grain boundaries, rendering these sites significantly more reactive than the bulk grains. Evidence for this comes from unpublished work on UO_2 single crystals, which do not show electrochemical activity in this potential region /J D Rudnicki; R E Russo and D W Shoesmith, unpublished data/.

At potentials more positive than $-0.4\ V_{SCE}$, the oxidation behaviour becomes irreversible /Shoesmith et al, 1994/. Thus, the charge associated with oxidation processes is not equal to the reduction charge and the photocurrent signal on the reduction scan differs from that during the oxidation scan in photoelectrochemical experiments. In this potential region, O^{2-} ions become incorporated in the UO_2 lattice, accompanied by the oxidation of U(IV) to U(VI) (or U(V)). Oxidation occurs more generally over the surface and is no longer restricted to active sites at grain boundaries. The anodic dissolution of the surface, i.e., dissolution of UO_2 as oxidized U(VI) species, has been shown to occur at $E > -0.3\ V_{SCE}$ /Shoesmith et al, 1996/. The surface becomes increasingly oxidized with increasing potential, until at $E = -0.1\ V_{SCE}$, the surface composition corresponds to $UO_{2.33}$ (U_3O_7). Although there is more general oxidation of the entire surface than at lower potentials, there may well still be some localization of the oxidation of the surface, with grain boundaries again tending to be more active sites. Because, on average, the surface composition corresponds to $UO_{2.33}$ at $-0.1\ V_{SCE}$, however, this potential is taken to the threshold potential for the oxidative dissolution of UO_2 /Shoesmith et al, 1994/.

In this study, the extent of oxidation of the UO_2 surface was limited. In relatively few experiments did E_{CORR} exceed the threshold potential for irreversible oxidation of $-0.4\ V_{SCE}$. Thus, in the majority of experiments, oxidation was limited to the oxidation of specific active surface sites, thought to be located at grain boundaries. This may account for the poor reproducibility observed in Figure 3-6, where the potentials recorded in H_2 atmospheres differ by up to 0.4 V. Polishing between experiments with 600-grit SiC

paper (grit size ~25 mm) could remove a surface layer several grains thick (grain size ~10 mm). Thus, the grain boundary structure would differ significantly from one experiment to the next.

Overall, there was less oxidation in irradiated H_2-containing environments, than in either Ar-containing solutions or in unirradiated H_2-containing environments. Thus, (i) the most negative E_{CORR} values were obtained in irradiated H_2 solutions (Figures 3-2 and 3-4), (ii) E_{CORR} decreased in experiments in which the gas was changed from Ar to H_2 or increased when changing from H_2 to Ar (Figure 3-5), (iii) E_{CORR} was lower in irradiated as opposed to unirradiated H_2-containing solutions (Figure 3-4), (iv) the initial oxidation rate was lowest in irradiated H_2 environments (Table 3-2), and (v) in the presence of radiation, the U(VI):U(IV) ratio was lower in H_2 than in Ar solutions.

An important observation from this work is that not only does the presence of H_2 suppress the oxidation of UO_2 in the presence of γ-radiation, but it also induces reduction in the extent of surface oxidation. The evidence for this conclusion comes from the fact that the final E_{CORR} values observed in irradiated H_2 solutions are lower than those in either unirradiated H_2- or Ar-containing solutions (Figures 3-1 and 3-4). Thus, H_2 not only consumes the oxidants produced by radiolysis but also reduces the surface as well, presumably through reaction between the surface and reducing radiolysis products such as e^-(aq) or H•. The present results are consistent with those of Sunder et al /1990/ who also found that H_2 reduced the rate of dissolution in α-irradiated experiments at 100°C below that observed in the absence of irradiation.

The exact nature of the effect of H_2 on the reduction of the UO_2 surface in irradiated environments in unknown. Because the majority of oxidation appears to be occurring at the specific active sites associated with reversible oxidation below a potential of –0.4 V_{SCE}, it is possible that radiolytic reductants can either suppress the oxidation of these sites (since the rate of initial oxidation is slowest for irradiated H_2 solutions, Table 3-2) or subsequently reduce these sites if they become oxidized (Figure 3-5). It is interesting to note that the addition of H_2 to an irradiated solution that was previously over-pressurized with Ar can drive the E_{CORR} from the irreversible oxidation regime (i.e., E > -0.4 V_{SCE}) to the reversible oxidation region (E < -0.4 V_{SCE}). Thus, in Figure 3-5, the E_{CORR} value in experiments SKB9 and 12 initially exceeded the irreversible threshold of –0.4 V_{SCE} in the presence of Ar, but then decreased well below this value when the Ar was replaced by H_2. This observation suggests that either the threshold for "irreversible" oxidation is more positive than previously believed or that reaction with radiolytic reductants leads to the removal of O^{2-} from the oxidized lattice. It can also be seen in Figure 3-5 that once reduced by the presence of H_2, the surface active sites only slowly oxidized if the H_2 was subsequently exchanged for Ar. From the results of experiments SKB8 and 10, it appears that a steady-state E_{CORR} of < -0.4 V_{SCE} is achieved in irradiated Ar-containing solution, 0.13–0.24 V more negative than that observed in Ar-containing solution not previously exposed to H_2 (SKB11 and 13).

Although the absolute values of E_{CORR} were variable in the various experiments in H_2-containing irradiated solutions, the trends observed were quite consistent. In experiments SKB6, 7, 8 and 10, E_{CORR} was observed to reach a maximum value after 100–400 min, followed by a subsequent decrease of several hundred mV. The results of these four experiments are shown in Figure 4-1, in which the difference in the absolute value of E_{CORR} has been corrected. The results of the four experiments are now seen to very reproducible, with a suppression of E_{CORR} of ~200 mV from the peak value after ~22 h exposure. Steady state had not been achieved in some of the experiments, suggesting that the surface would eventually become even more reduced.

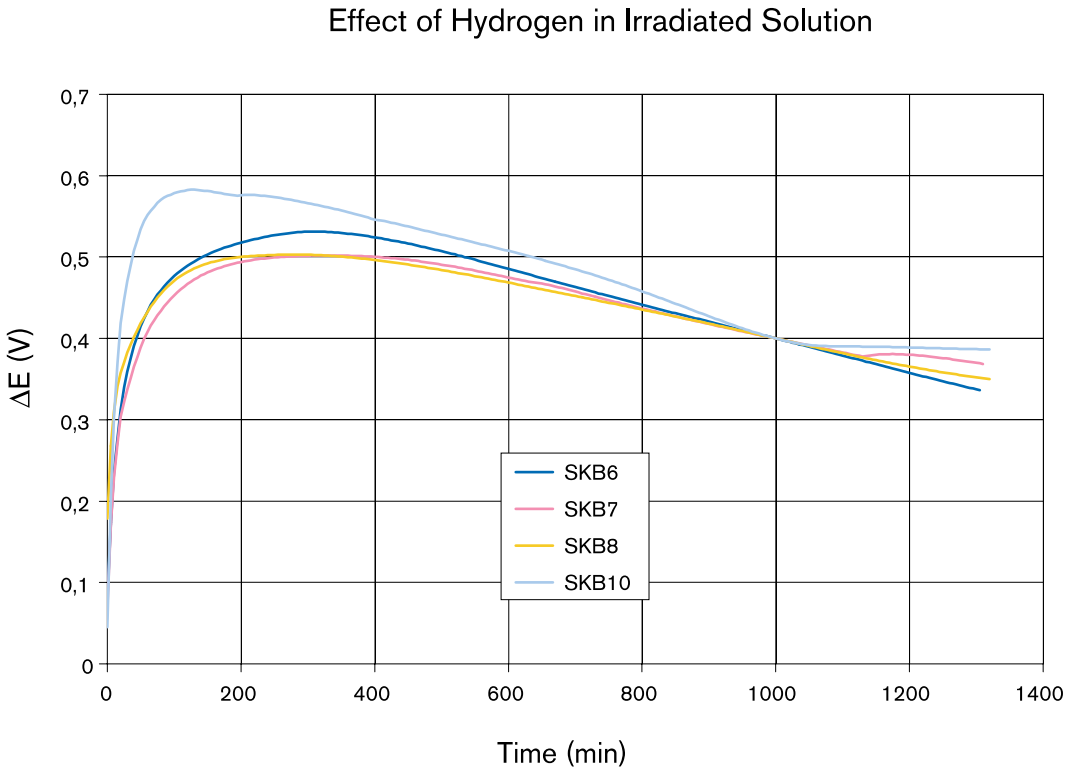

Figure 4-1. *Magnitude of the effect of H_2 in irradiated solution.*

The kinetics of reactions in irradiated H_2 environments appear to be more sluggish than in other environments. Thus, the rate of initial oxidation was slower, on average, in experiments SKB5, 6, 7, 8 and 10 than in either unirradiated solutions or irradiated Ar environments (Table 3-2). In addition, the rate of attainment of steady-state was slower in irradiated H_2 solutions, if indeed steady state can be said to have been achieved in the duration of the experiments (Figures 3-2 and 3-4). The effect of H_2 on the kinetics of UO_2 oxidation are also seen once the H_2 has been removed from the system and replaced by Ar. The rate of increase in E_{CORR} in the second half of experiments SKB8 and SKB10 (Figure 3-5) is slower, and the ultimate steady-state E_{CORR} lower, than that observed if the electrode is exposed to an Ar atmosphere without prior exposure to H_2. Thus, the surface reactions in the H_2 atmosphere have reduced the active surface sites to such a degree that their subsequent re-oxidation is hindered.

As discussed in more detail below, the kinetics of reactions in irradiated H_2 environments would be expected to be dependent upon both the H_2 partial pressure, temperature and the nature and magnitude (dose rate) of the irradiation. This may account for the reason why no effect was observed of the H_2 produced radiolytically in Ar-containing solution in experiment SKB13. Approximately 0.01 MPa (1.6 psi) H_2 was formed in this experiment, yet E_{CORR} appears to have attained steady state with no indication of a subsequent decrease (Figure 3-3). Furthermore, the absolute value of the steady-state E_{CORR} is more positive than that observed in experiment SKB11 in which no H_2 was found.

There are a number of literature studies with which the present data can be compared. Sunder and Miller /S Sunder and N H Miller, unpublished work/ studied the effect of H_2 and Ar on the oxidation of UO_2 in the presence of γ-radiation in deaerated 0.1 mol·dm^{-3} $NaClO_4$ (pH 9.5) in the same facility used in the present studies. The gases were used at atmospheric pressure at room temperature. The same facility was also used by Sunder et al /1992/ to study the effect of γ-radiolysis on the oxidation of UO_2 in a variety of en-

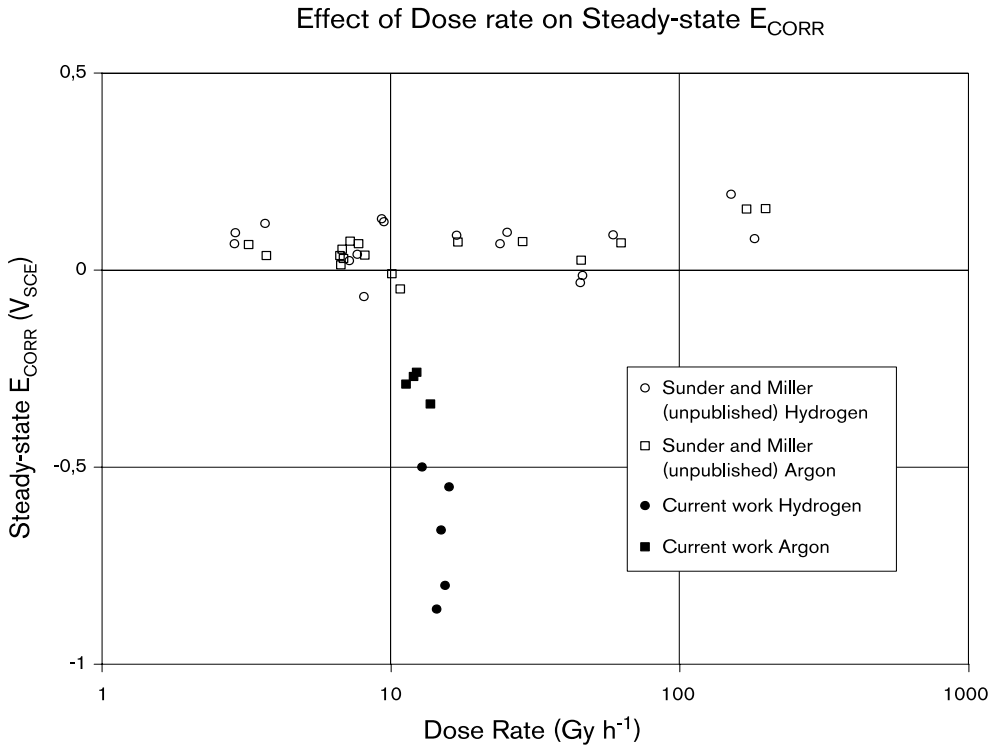

Figure 4-2. *Effect of dose rate on the corrosion potential of UO_2 in γ-irradiated solution. Current work – solid symbols (● H_2 ■ Ar), Sunder and Miller /unpublished data) – open symbols (O H_2 □ Ar).*

vironments chosen to favour the formation of different radical species. In both studies, a combination of E_{CORR} measurements, CSV and XPS were used to determine the extent of dissolution, as in the present study. Finally, Sunder et al /1990/ studied the effect of H_2 on the dissolution of UO_2 in H_2O in the presence of α-radiation at a temperature of 100°C, using a combination of solution analyses for dissolved U and XPS.

Figure 4-2 compares the steady-state E_{CORR} values determined by Sunder and Miller /unpublished data/ as a function of dose rate with those measured in this study. In both studies, the solutions were in contact with either H_2 or Ar, at a pressure of either 5 MPa (this study) or 0.1 MPa /Sunder and Miller/. There are two obvious differences between the two sets of data. First, Sunder and Miller observed no difference in behaviour between the two gases, whilst the results of the current work gave more negative potentials with H_2. Second, the E_{CORR} values with Ar from the current study are several hundred millivolts more negative than those observed by Sunder and Miller at a similar dose rate.

The absence of an observed effect of H_2 in the Sunder and Miller study may be related to the kinetics of the reactions with reducing radiolysis species. If the concentration of active species is proportional to the $[H_2]$, then on simple first-order kinetic considerations the rate of reaction could be fifty times slower at 0.1 MPa partial pressure than with 5 MPa. As it is, the kinetics have been found to be sluggish even at a H_2 partial pressure of 5 MPa (see above).

The more negative E_{CORR} values in Ar-purged solutions in the current study are more difficult to explain. The possible causes include: (i) an effect of pressure, (ii) differences in the surface reactivity of the UO_2 electrodes, and (iii) a difference in the behaviour in $NaClO_4$ and NaCl solution. First, since the oxidation of UO_2 does not involve large volume changes and since Ar is assumed to be inert in the presence of γ-radiation, the

partial pressure of Ar would not be expected to affect the rate or extent of oxidation. Second, two different UO_2 electrodes were used in the current study and, at least where comparison is possible, gave similar results (Figure 3-6). It is possible that the Sunder and Miller data were measured using an electrode manufactured from a particularly reactive piece of UO_2, accounting for the more positive E_{CORR} values in Ar-purged solutions in their study. However, if this were so, the enhanced reactivity appears to mask any difference between the behaviour in Ar and H_2.

The final possibility is a difference due to the nature of the electrolyte. The significant difference between the two electrolytes is the degree to which they participate in radiolysis reactions. Perchlorate is considered to be inert for the purposes of radiolysis modelling, whereas Cl^- participates in a large number of radiolysis reactions /Sunder and Christensen, 1993/. Despite this difference, however, the predicted concentrations of H_2 and $e^-(aq)$ in the two solutions are virtually identical. Most of the additional species formed in Cl^-- containing solution (such as ClO_2, Cl_2 and $HClO_3$) would be expected to be oxidants rather than reductants, and, hence, would tend to give more positive E_{CORR} values rather than the more-negative values observed here. Unfortunately, Sunder and Christensen /1993/ do not give the relative concentrations of H• in the two solutions. This reductant is formed by the following reactions:

$$OH\bullet + H_2 \rightarrow H\bullet + H_2O \quad (1)$$

$$e^-(aq) + H^+ \rightarrow H\bullet \quad (2)$$

and

$$e^-(aq) + H_2O \rightarrow H\bullet + OH^- \quad (3)$$

and is a primary species produced by γ-radiolysis with a G-value of 0.55 molecules/ 100 eV /Christensen and Sunder, 1998/. Once formed, H• participates in a number of reactions with other radical and molecular species /Sunder and Christensen, 1993/. The rate of Reaction (1) increases with the partial pressure of H_2 and could have resulted in higher [H•] in the present study. However, there is no supporting evidence to suggest that H• is the active reducing species in this study.

Figure 4-3 compares the dependence of the U(VI):U(IV) ratio on the steady-state E_{CORR} in γ-irradiated solution from the current study with those found by Sunder and Miller /unpublished data/ and Sunder et al /1992/. These latter two studies were conducted at various dose rates in order to produce a range of oxidizing environments. The Sunder et al /1992/ studies were conducted in a number of different solutions designed to produce specific radical or molecular oxidants. Despite the difference in environments and the difference in reactivity of the UO_2 electrodes, the data from the current study are consistent with those from the earlier work. Only minor oxidation of the surface is observed at $E_{CORR} < -0.1\ V_{SCE}$, with increasing U(VI):U(IV) ratios above this potential. This figure also emphasizes the significantly more negative potentials observed in this study in environments containing 5 MPa H_2 (the full circles in Figure 4-3).

The study of Sunder et al /1990/ suggests that the effects of H_2 observed in this study are also found in α-irradiated solutions. In the Sunder et al /1990/ study, the extent of dissolution of UO_2 as a result of α-radiolysis was determined by both XPS and solution U analyses. Nitrogen, 10%H_2/N_2 and 100% H_2 were passed through the autoclave containing the UO_2 at a partial pressure of 0.1 MPa and at a temperature of 100°C. Hydrogen suppressed the oxidation of UO_2 (as measured by the U(VI):U(IV) ratio) compared with the behaviour in N_2, with 10%H_2/N_2 producing intermediate results. Furthermore, with 100% H_2, the dissolved [U] and U(VI):U(IV) ratio were lower in the presence of α–radiolysis than with no irradiation. This latter observation is consistent

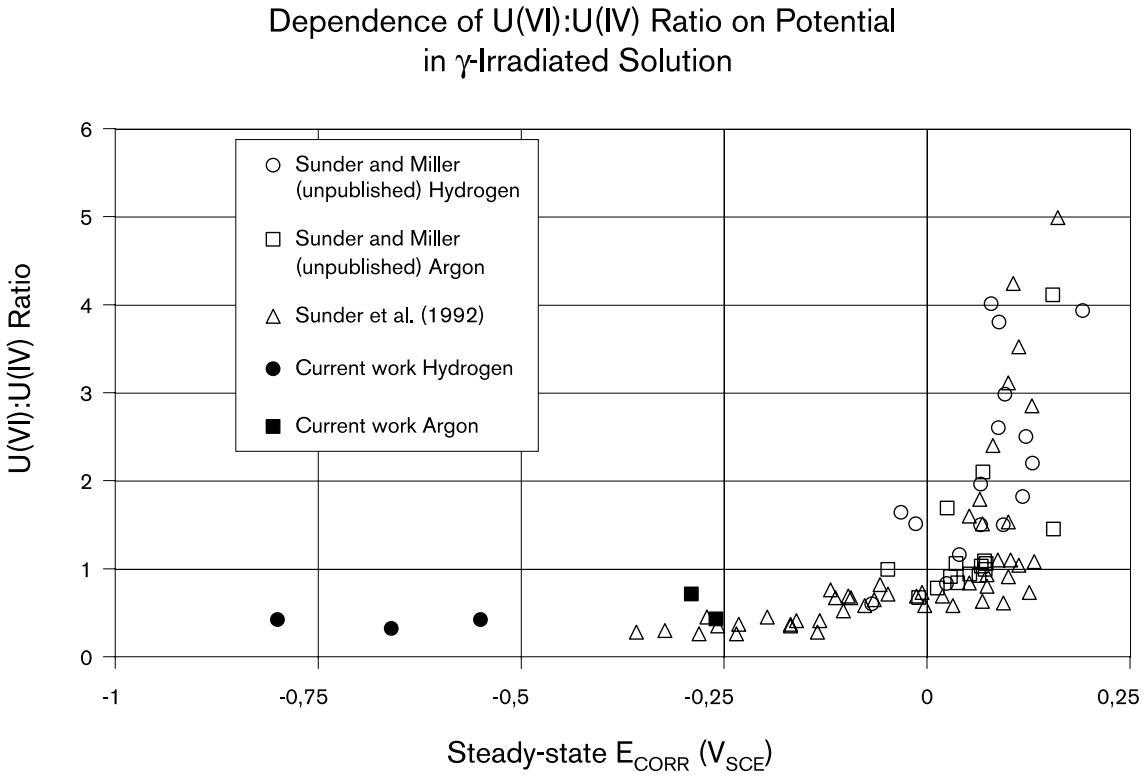

Figure 4-3. *Dependence of U(VI):U(IV) ratio on potential in γ-irradiated solution. Current work – solid symbols (● H_2 ■ Ar), Sunder and Miller /unpublished data/ – (O H_2 □ Ar), Sunder et al /1992/ (Δ).*

with the observation in the current work that not only does the presence of H_2 suppress the effects of radiolytic oxidants, but it also drives the environment more reducing than in an unirradiated solution.

The results of the Sunder et al /1990/ work indicate that H_2 can suppress the radiolytically-induced oxidation of UO_2 at low [H_2] at elevated temperature. Thus, suppression of oxidation was observed at [H_2] as low as ~$1.6 \cdot 10^{-4}$ mol·dm^{-3} (equivalent to a partial pressure of ~0.01 MPa). This H_2 partial pressure was insufficient to suppress oxidation due to γ-radiolysis at room temperature, either in the Sunder and Miller /unpublished data/ study (H_2 partial pressure 0.1 MPa) or the current study (experiment SKB13, H_2 partial pressure ~0.01 MPa). This suggests that elevated temperature can offset the effects of lower H_2 partial pressures, possibly because of the effect of temperature on the kinetics of the process.

In previous studies of the effect of γ-radiation on the dissolution of UO_2, the dissolution (corrosion) rate has been estimated from the measured E_{CORR} values /Johnson et al, 1996; Shoesmith and Sunder, 1991/. In those studies, E_{CORR} values in excess of the oxidative threshold of –0.1 V_{SCE} were observed /Sunder et al, 1992/, a potential above which the surface can be considered to be uniformly dissolving. In the present study, however, the measured E_{CORR} were more negative and, in the case of experiments in which E_{CORR} < -0.4 V_{SCE}, indicative of very localized oxidation on the surface. Therefore, application of the Shoesmith-Sunder electrochemical dissolution model is inappropriate for the present data.

The results of the current study indicate an effect of H_2 in suppressing the oxidation of UO_2, but leave several questions unanswered. First, the mechanism of the process is

unclear. The most likely mechanism involves the reaction of reducing radiolysis species both in solution and at the UO_2 surface. The relative predominance of radiolytic oxidants and reductants may be significantly different in H_2-containing solutions at elevated H_2 partial pressure from that in Ar-containing solution. In addition, however, it appears that surface reactions are important in driving the surface to a highly reduced state, particularly at the reactive grain boundary locations. A series of radiolysis calculations to determine the effect of H_2 on the distribution of oxidants and reductants in the presence of α- and γ-radiation may be helpful in identifying the active reducing species in this system. Calculations should be performed as a function of H_2 partial pressure for both $NaClO_4$ and NaCl solutions. Experiments on UO_2 single crystals may also indicate whether H_2 has a similar effect in suppressing the oxidation of the body of the UO_2 grains, as it appears to do at the grain boundaries. The second major question is that of the kinetics of the reactions between H_2 and UO_2 oxidation. There is evidence to suggest that H_2 can suppress UO_2 oxidation due to radiolysis at high $[H_2]$ at ambient temperature and at low $[H_2]$ at elevated temperature. The exact dependence of the process of $[H_2]$ and temperature, however, is unknown.

The results of the current and previous studies on UO_2 have a number of implications for the behaviour of used fuel. Both the current results and those of Sunder et al /1990/ indicate that H_2 not only suppresses the oxidation of UO_2 due to radiolytic oxidants, but it also reduces the extent of oxidation of the surface. Thus, the surface of used fuel that has become oxidized during service or storage could not only be prevented from further oxidizing during disposal, but could actually be reduced. From the relatively short-term results obtained here, it also appears that the effect of H_2 is persistent even once the H_2 has been removed from the system. Thus, it might be possible to pretreat used fuel in a H_2-containing environment prior to disposal in order to suppress oxidation in the disposal vault. Since the beneficial effect of H_2 has been reported for both α- and γ-radiation, it appears that a similar beneficial effect should be observed for fuel subject to α-, β- and γ-radiation. Finally, further studies are required to define the combination of $[H_2]$ and temperature necessary for this effect to be observed. In the current study, the amount of H_2 produced by radiolysis of the solution in short-term experiments (with a large solution volume:UO_2 surface area ratio) was insufficient to suppress oxidation at room temperature. At the elevated initial temperature of the fuel surface, however, smaller amounts of H_2 may produce the same effect.

5 Summary

The extent of oxidation of UO_2 by γ-radiolysis has been studied in deaerated 0.1 mol·dm^{-3} NaCl (pH 9.5) over-pressurized with either Ar or H_2 gas at a pressure of 5 MPa. Hydrogen is found to not only suppress oxidation due to radiolytic oxidants but also to reduce the extent of surface oxidation observed in either Ar of H_2 atmospheres in the absence of radiation. This dual effect of H_2 is most likely the result of reactions between reducing species and both oxidants in solution and reactive surface sites, the latter possibly located at grain boundaries. The nature of the reducing species responsible for these effects cannot be identified on the basis of the current data.

The effects of H_2 have been found to be kinetically slow (compared with the rate of oxidation in Ar) and persistent, retarding the subsequent re-oxidation of the surface after the H_2 atmosphere has been replaced by Ar.

Further work is required to define the range of conditions of [H_2] and temperature over which oxidation of the UO_2 surface is suppressed by H_2.

References

Christensen H, Sunder S, 1998. Current state of knowledge in radiolysis effects on spent fuel corrosion. Studsvik Material Report, STUDSVIK/M-98/71.

Eriksen T, 1996. Radiolysis of water within a ruptured fuel element. SKB PR U-96-29, Svensk Kärnbränslehantering AB.

Hocking W H, Betteridge J S, Shoesmith D W, 1991. The cathodic reduction of dioxygen on uranium dioxide in dilute alkaline aqueous solution. Atomic Energy of Canada Limited Report, AECL-10402.

Johnson L H, LeNeveu D M, King F, Shoesmith D W, Kolar M, Oscarson D W, Sunder S, Onofrei C, Crosthwaite J L, 1996. The disposal of Canada's nuclear fuel waste: A study of postclosure safety of in-room emplacement of used CANDU fuel in copper containers in permeable plutonic rock: Volume 2: Vault model. Atomic Energy of Canada Limited Report, AECL-11494-2, COG-96-552-2.

Shoesmith D W, Sunder S, 1991. An electrochemistry-based model for the dissolution of UO_2. Atomic Energy of Canada Limited Report, AECL-10488.

Shoesmith D W, Sunder S, Hocking W H, 1994. Electrochemistry of UO_2 nuclear fuel. In: The Electrochemistry of Novel Materials, (Editors J Lipkowski and P N Ross), VCH, New York, NY, p. 297–337.

Shoesmith D W, Tait J C, Sunder S, Gray W J, Steward S A, Russo R E, Rudnicki J D, 1996. Factors affecting the differences in reactivity and dissolution rates between UO_2 and spent nuclear fuel. Atomic Energy of Canada Limited Report, AECL-11515, COG-95-581.

Sunder S, Boyer G D, Miller N H, 1990. XPS studies of UO_2 oxidation by alpha radiolysis of water at 100°C. Journal of Nuclear Materials 175, 163–169.

Sunder S, Shoesmith D W, Christensen H, Miller N H, 1992. Oxidation of UO_2 fuel by the products of gamma radiolysis of water. Journal of Nuclear Materials 190, 78–86.

Sunder S, Christensen H, 1993. Gamma radiolysis of water solutions relevant to the nuclear fuel waste management program. Nuclear Technology 104, 403–417.

Appendix A:

Detailed operating procedures for purging and over-pressurizing vessel with Ar and H_2 gas

The gas train attached to the pressure vessel is shown schematically in Figure 2-2 of the main text.

1 Deaeration with Ar prior to experiment

Deaeration of the test solution was achieved by flowing Ar from the Ar deaeration cylinder through the pressure vessel at atmospheric pressure through open valves A, B, C and E (valve D closed). Deaeration was performed for 30 min prior to each experiment and for the 5–10 min duration of the electrode cathodic cleaning step.

2 Over-pressurization with Ar gas

The gas line between the Ar over-pressurization cylinder and valve D was first flushed to remove air. With valves A and E closed and valves B, C and D open, the pressure vessel was slowly over-pressurized with 5.2 MPa (750 psi) Ar. Valve D was then closed, and the pressure monitored during the experiment using the pressure gauge.

The ^{192}Ir source was then extended into the irradiation chamber, if necessary.

3 Over-pressurization with H_2 gas

Following deaeration with Ar, the H_2 supply line between the cylinder and valve D was flushed with H_2 to remove atmospheric O_2 (valve C closed, valves D and E open). Valve E was then closed and the pressure vessel slowly filled with ~5.2 MPa (~750 psi) H_2 by opening valves B and C. Initially, therefore, the pressure vessel contained ~0.1 MPa (~15 psi) Ar and ~5.1 MPa (~730 psi) H_2. It was assumed that Ar is inert in the presence of γ-irradiation. Because of the tendency for H_2 to leak from the system, it was found necessary to keep valve D open throughout the experiment.

The ^{192}Ir source was then extended into the irradiation chamber, if necessary.

4 Switching from Ar to H_2

Valve C was first closed to isolate the pressure vessel. The line between the H_2 cylinder and valve D was then pre-flushed through valve E. Valve D was then closed to isolate the H_2 cylinder and the flushed line and the pressure vessel vented through valve E by opening valve C. The pressure inside the vessel was allowed to drop to ~0.1 MPa (~15 psi) before closing valve E. The pressure vessel was then slowly filled with ~5.2 MPa (~750 psi) H_2 by opening valve D. As with initial over-pressurization with H_2 gas, the vessel then contained ~0.1 MPa (~15 psi) Ar and ~5.1 MPa (~730 psi) H_2. Because of the tendency for H_2 to leak from the system, it was again found necessary to keep valve D open throughout the remainder of the experiment.

The ^{192}Ir source could remain extended into the irradiation chamber throughout this procedure, since neither of the valves attached directly to the pressure vessel (valves A and B) were operated.

5 Switching from H_2 to Ar

The line between the Ar over-pressurization cylinder and valve D was pre-flushed with Ar to remove air and valve D closed. The H_2 over-pressure in the vessel was relieved by opening valve C until the pressure had dropped to ~0.1 MPa (~15 psi). The ^{192}Ir source was then retracted and valve A opened and the dissolved H_2 removed from the solution by purging with Ar at atmospheric pressure through valve E for ~10 min. Valves A and E was then closed, and the source re-extended into the irradiation chamber. The pressure vessel was then slowly over-pressurized with ~5.2 MPa (~750 psi) Ar from the over-pressurization cylinder through the previously flushed line and valve D. Valve D was then closed. This procedure was adopted to remove all traces of H_2 prior the second part of the experiment.

6 Depressurization and degassing prior to CSV

The ^{192}Ir source was retracted. Valve D (if open) was closed and the pressure vessel vented through valve E to a pressure of ~0.1 MPa (~15 psi). Regardless of the nature of the over-pressurizing gas, the pressure vessel was then degassed with Ar through valve A for 30 min to remove H_2 or other radiolytically-formed gases prior to performing the cathodic-stripping voltammogram. After the CSV, valves A and B were closed to isolate the pressure vessel prior to its removal to the anaerobic chamber for disassembly.

Appendix B:

The time dependence of E_{CORR} for the thirteen individual experiments

Appendix B contains the individual time versus E_{CORR} plots for the thirteen experiments (SKB1–13) defined in Table 2-1 of the main text.

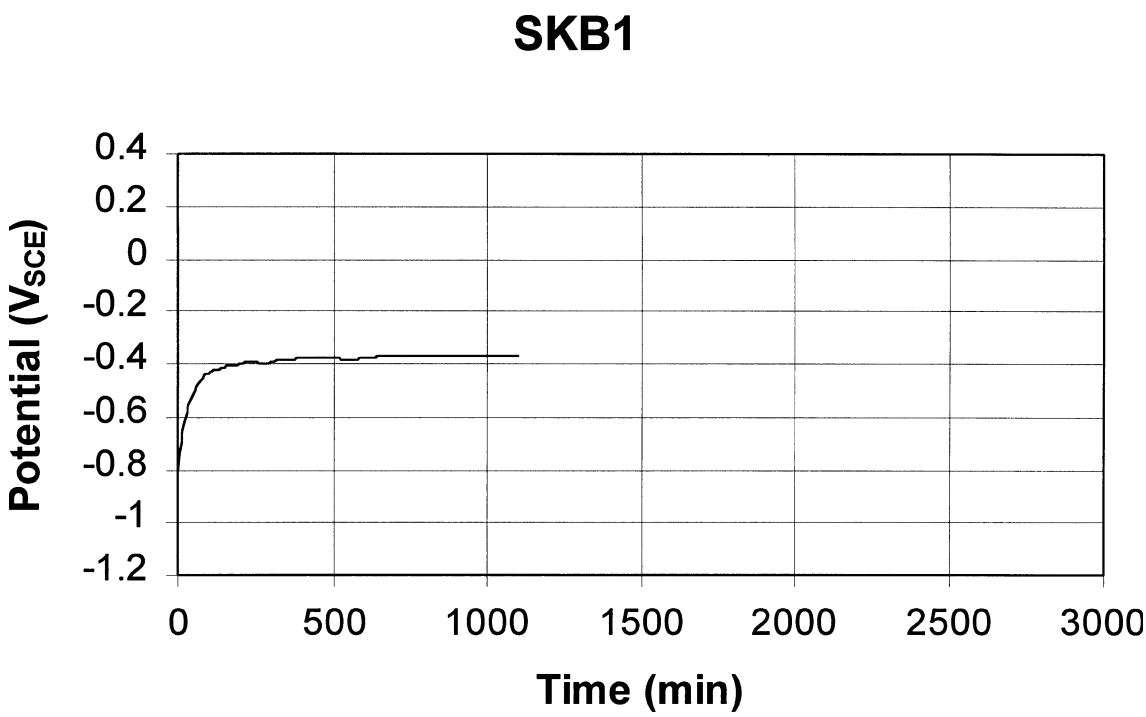

Figure B1. *Time dependence of E_{CORR} for experiment SKB1.*

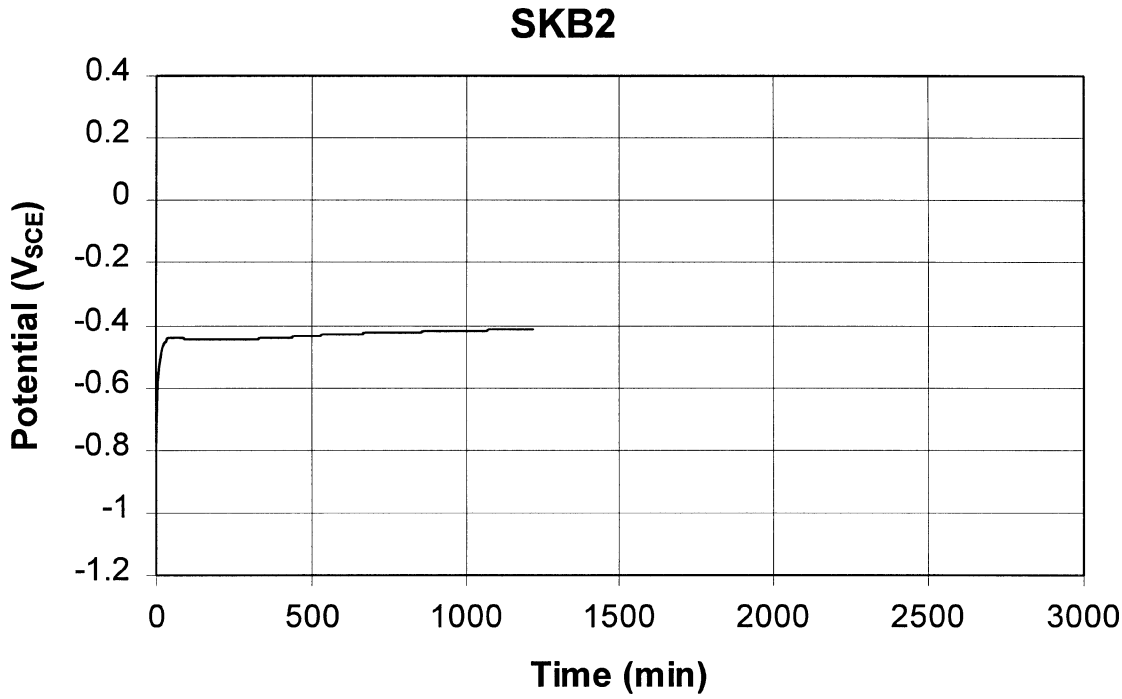

Figure B2. *Time dependence of E_{CORR} for experiment SKB2.*

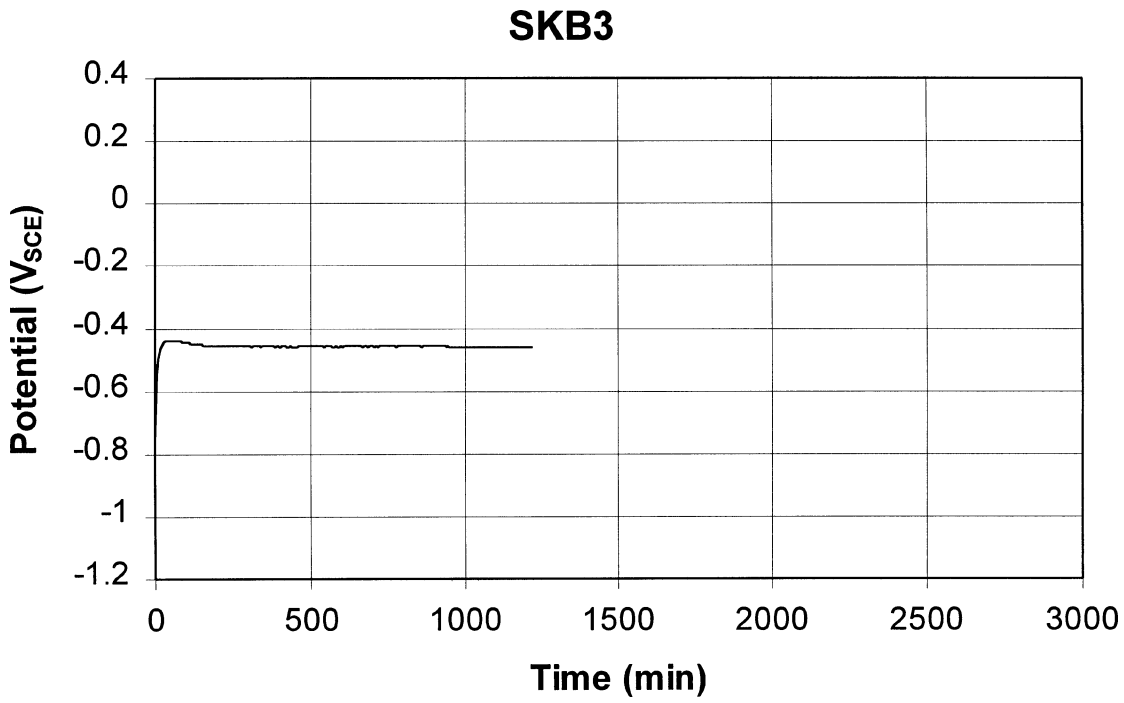

Figure B3. *Time dependence of E_{CORR} for experiment SKB3.*

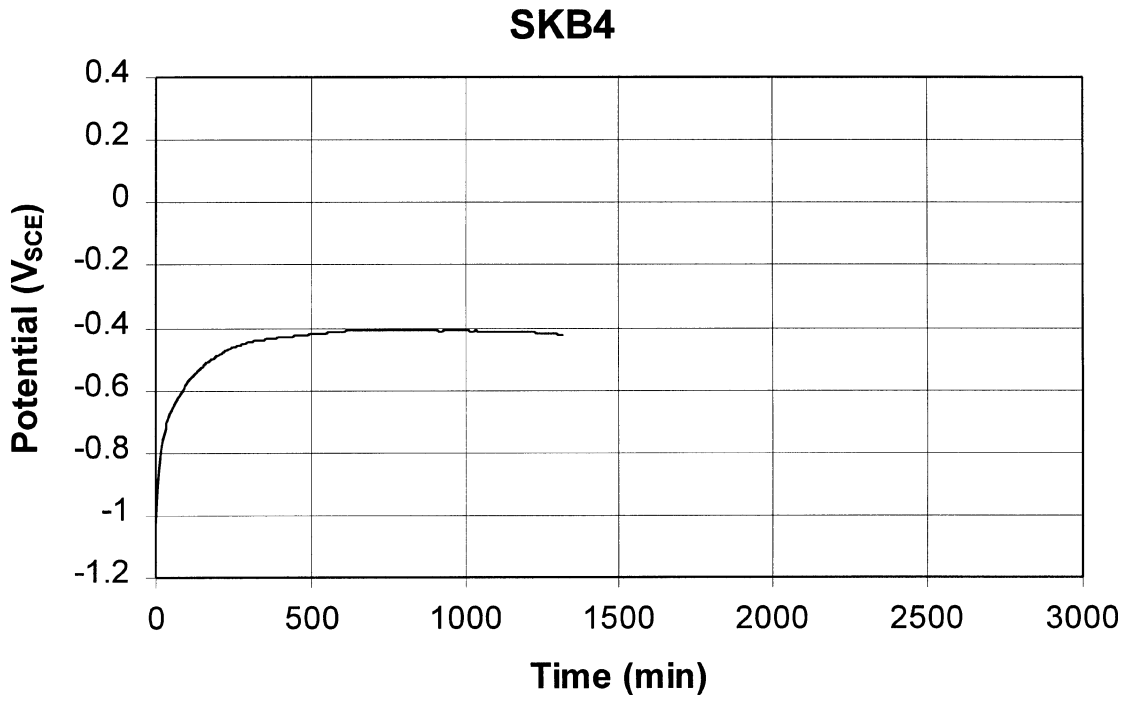

Figure B4. *Time dependence of E_{CORR} for experiment SKB4.*

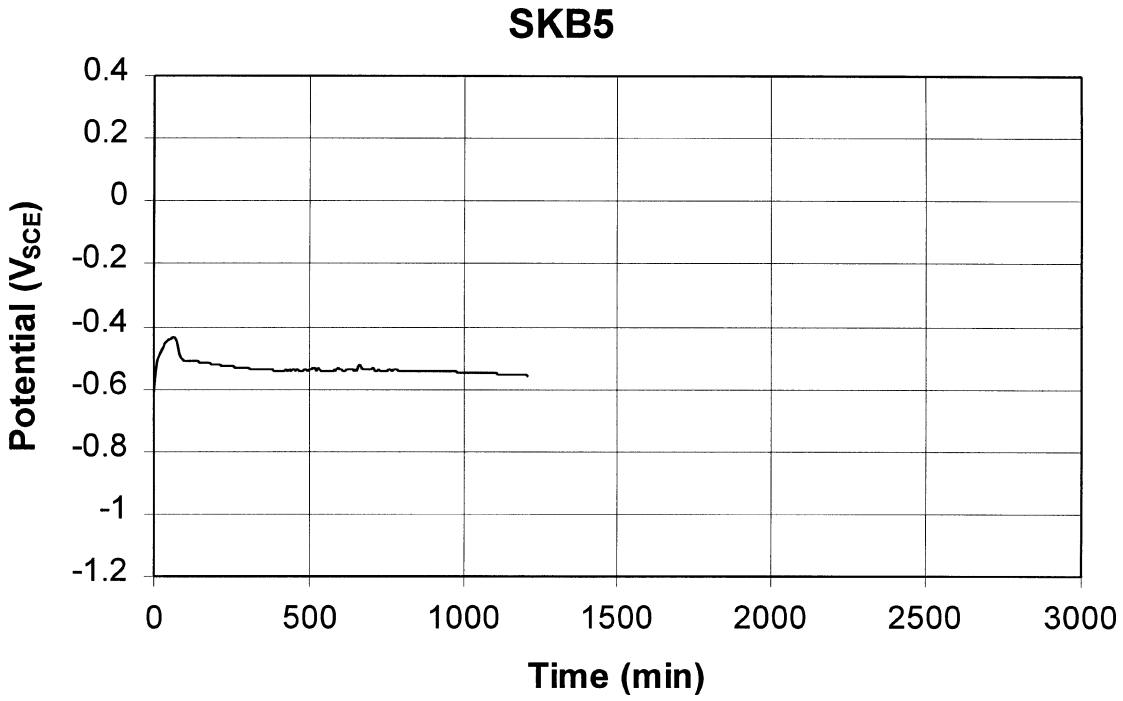

Figure B5. *Time dependence of E_{CORR} for experiment SKB5.*

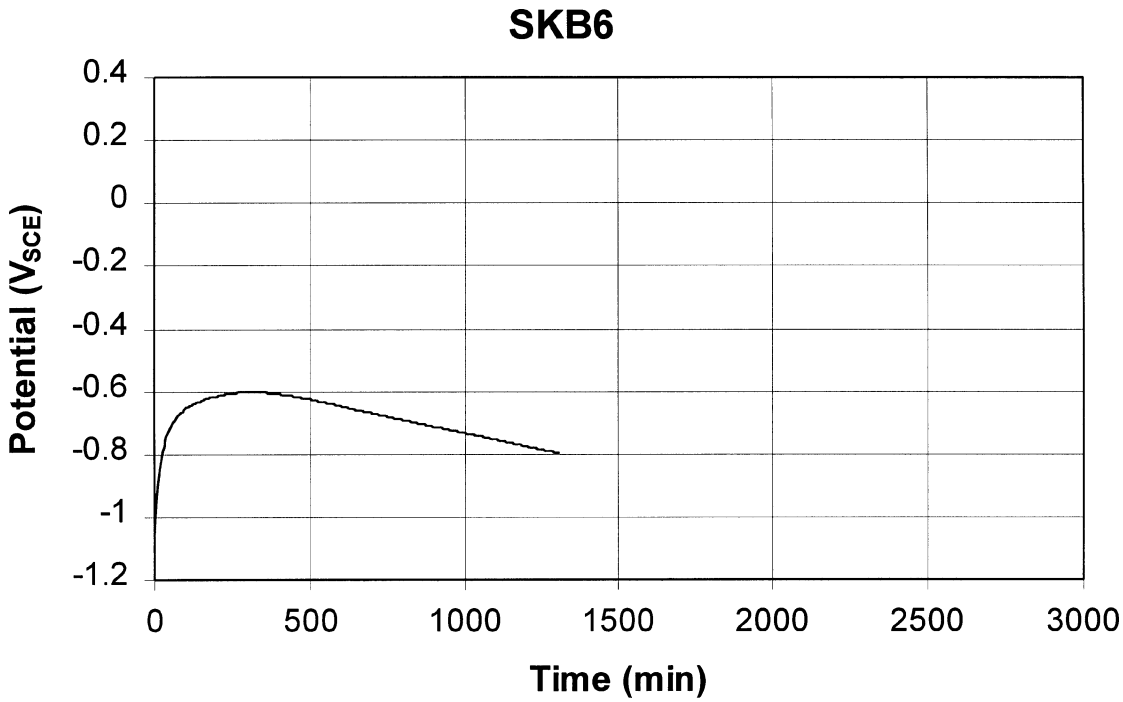

Figure B6. *Time dependence of E_{CORR} for experiment SKB6.*

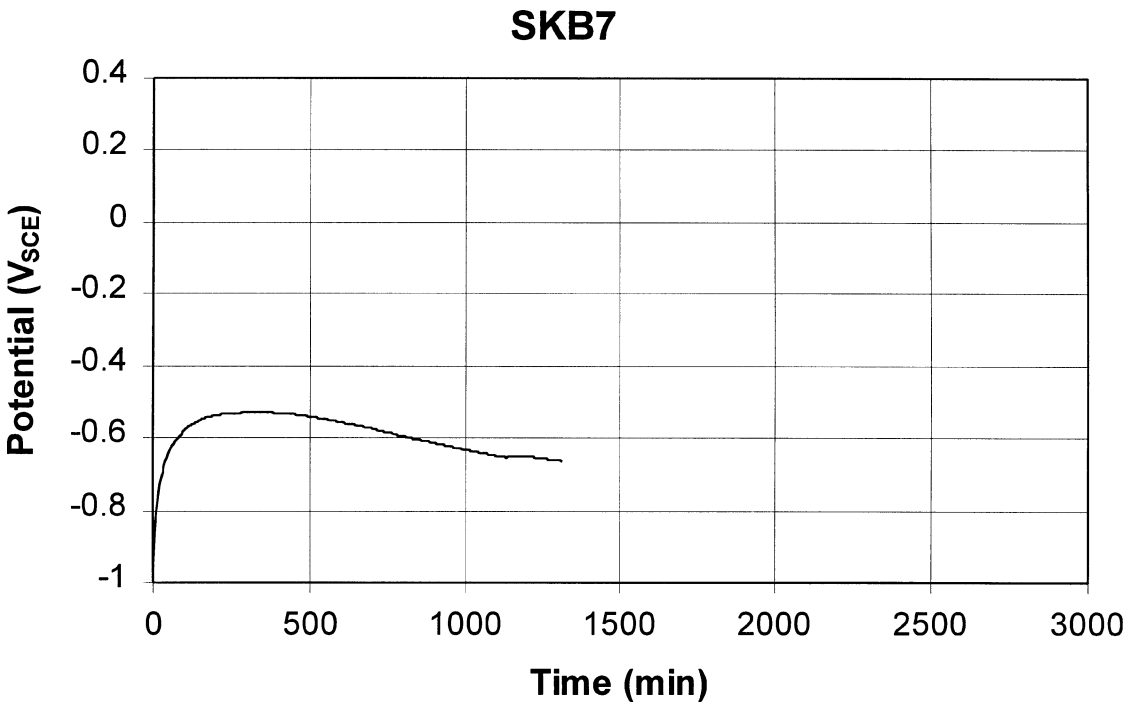

Figure B7. *Time dependence of E_{CORR} for experiment SKB7.*

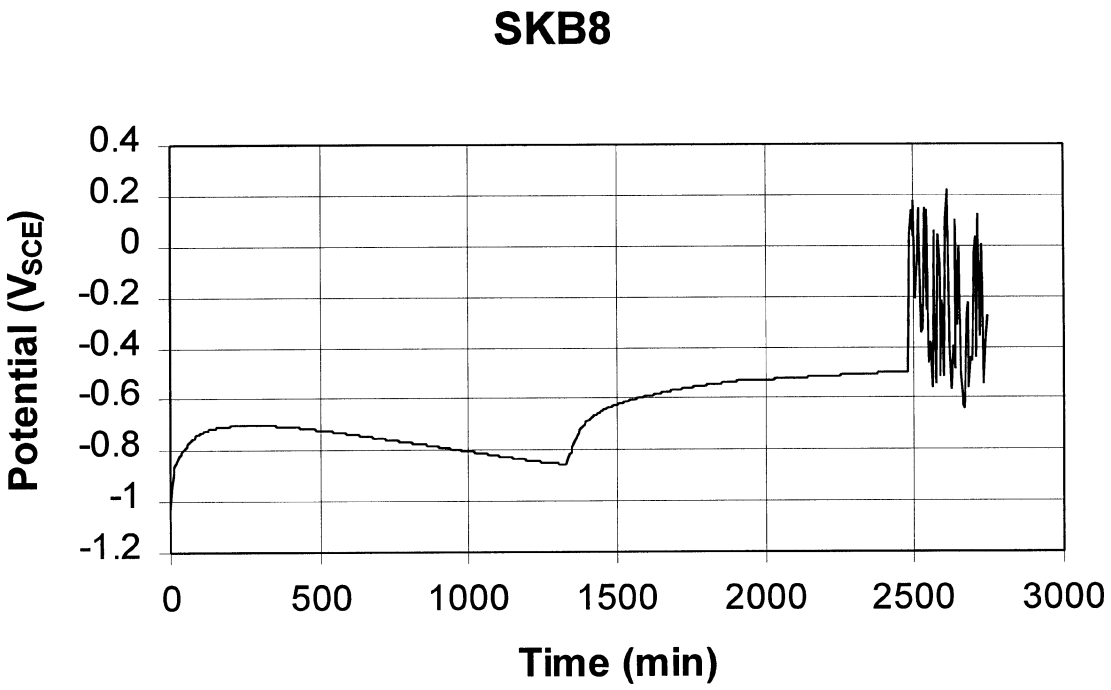

Figure B8. *Time dependence of E_{CORR} for experiment SKB8.*

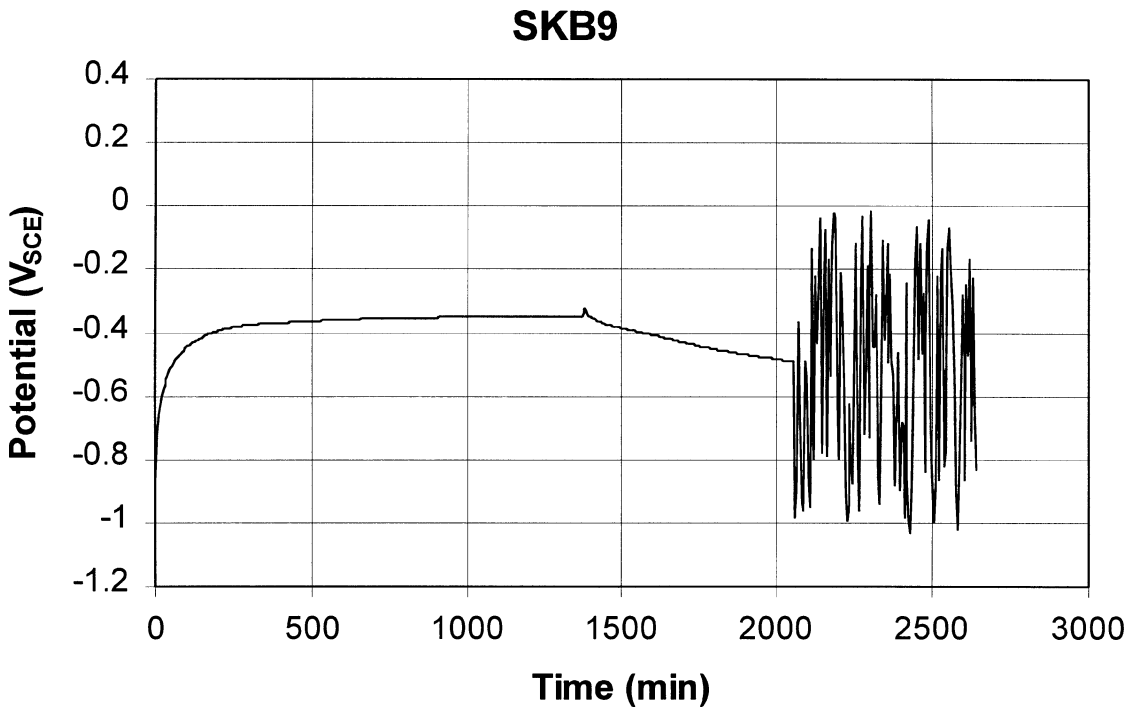

Figure B9. *Time dependence of E_{CORR} for experiment SKB9.*

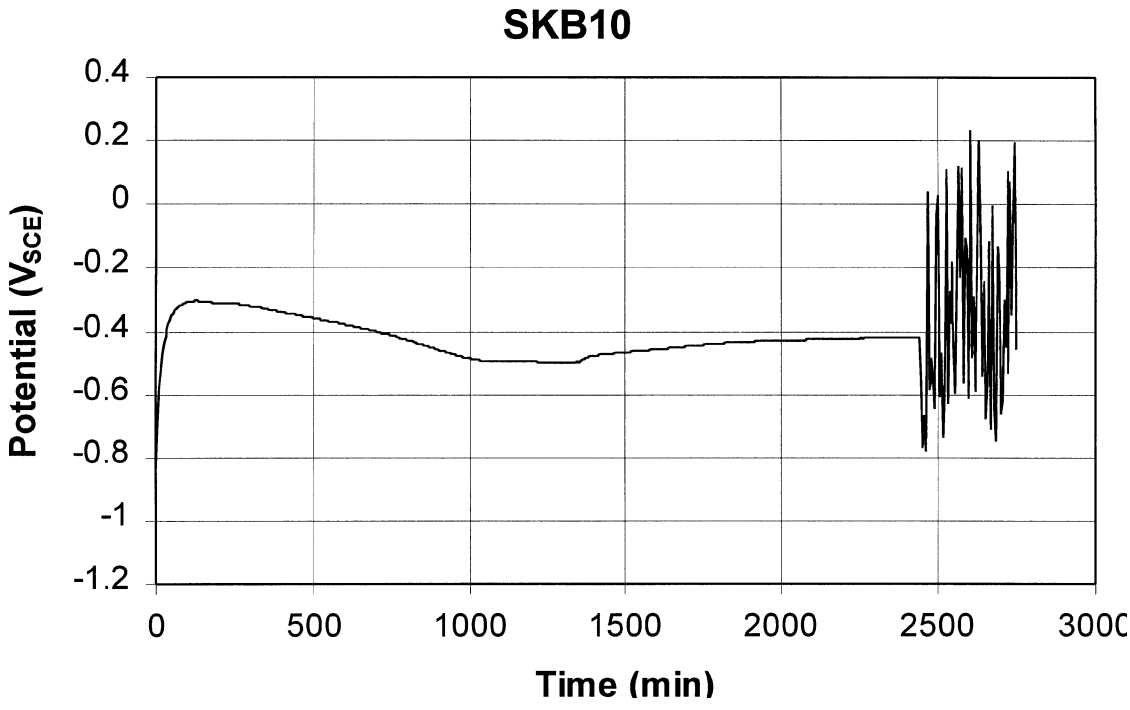

Figure B10. *Time dependence of E_{CORR} for experiment SKB10.*

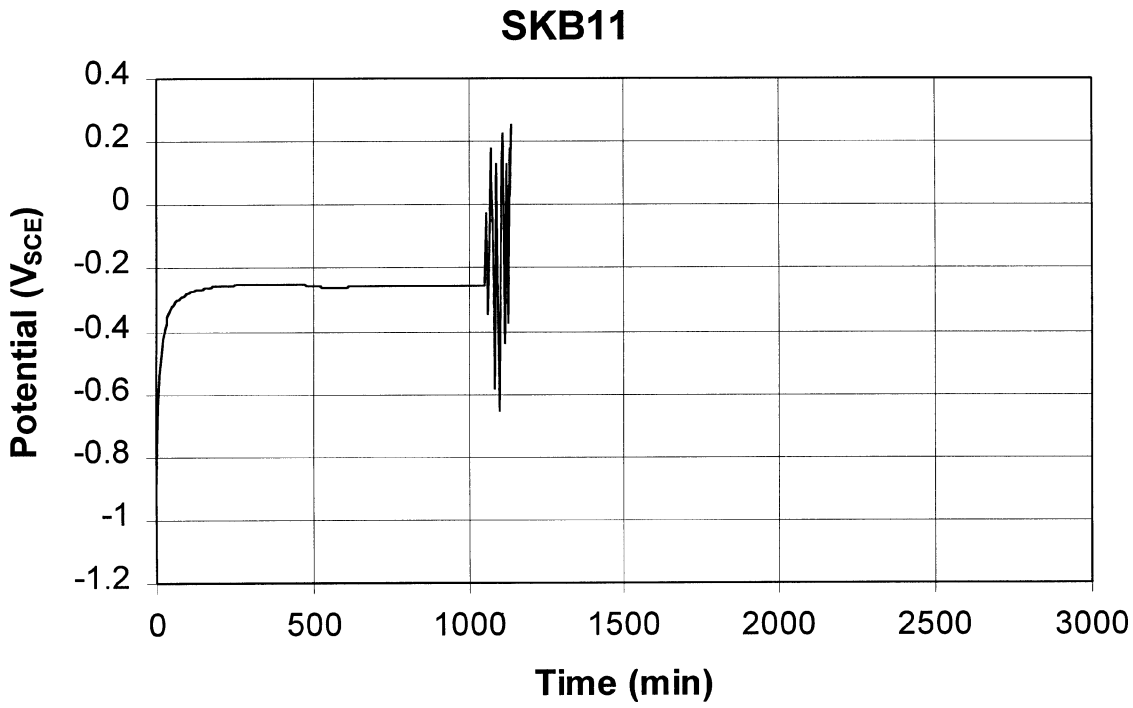

Figure B11. *Time dependence of E_{CORR} for experiment SKB11.*

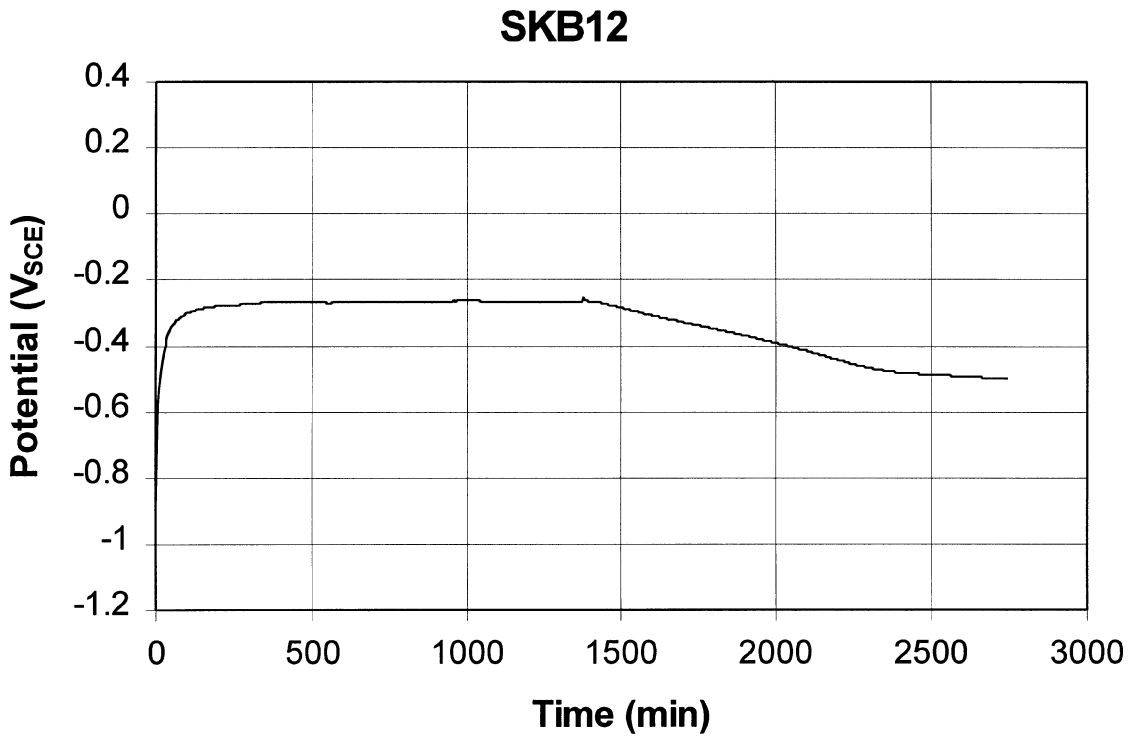

Figure B12. *Time dependence of E_{CORR} for experiment SKB12.*

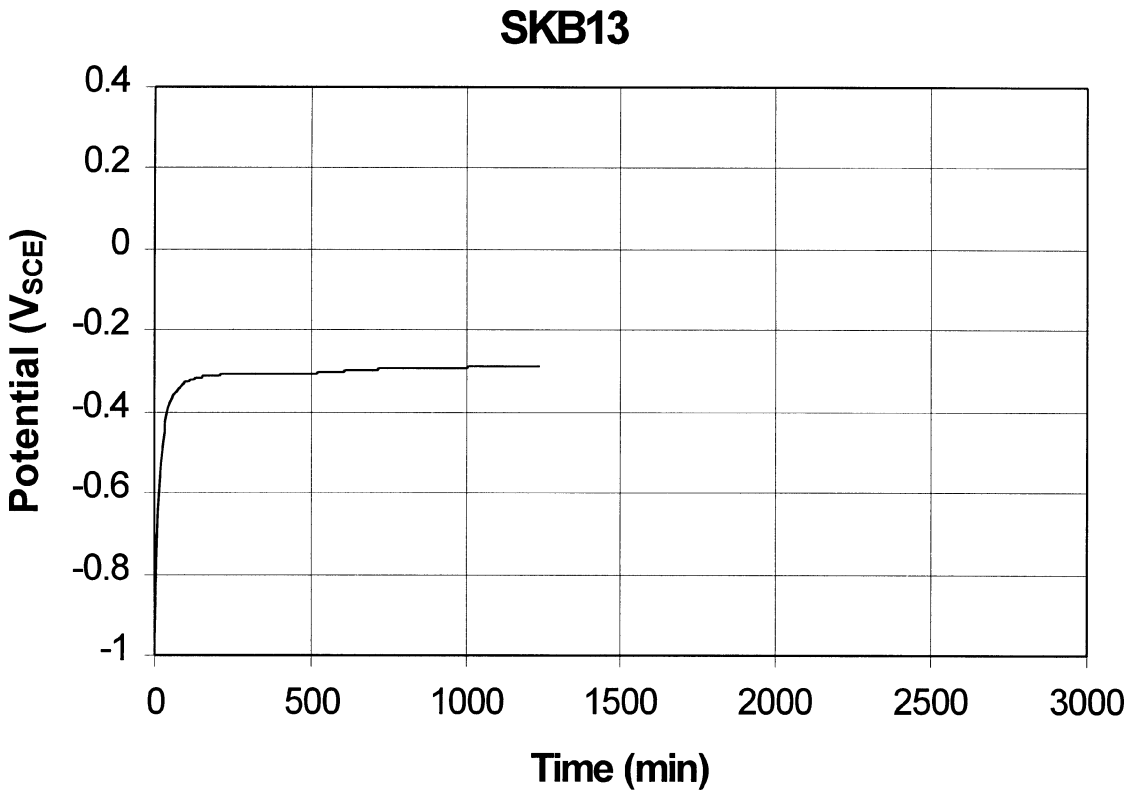

Figure B13. *Time dependence of E_{CORR} for experiment SKB13.*